UNIVERSIDADE FEDERAL FLUMINENSE

INSTITUTO DE GEOCIÊNCIAS

PROGRAMA DE PÓS-GRADUAÇÃO EM DINÂMICA DOS OCEANOS E DA TERRA

LAISA DA FONSECA AGUIAR

IDENTIFICATION OF BOTTOM SIMULATING REFLECTORS IN THE FOZ DO AMAZONAS BASIN, NORTHERN BRAZIL, USING SEISMIC AMPLITUDES, SEISMIC ATTRIBUTES AND FREQUENCY ANALYSIS

Niterói

2020

LAISA DA FONSECA AGUIAR

IDENTIFICATION OF BOTTOM SIMULATING REFLECTORS IN THE FOZ DO AMAZONAS BASIN, NORTHERN BRAZIL, USING SEISMIC AMPLITUDES, SEISMIC ATTRIBUTES AND FREQUENCY ANALYSIS

Dissertation submitted to the Programa de Pós-Graduação em Dinâmica dos Oceanos e da Terra of Universidade Federal Fluminense in partial fulfillment of the requirements for obtaining the degree of Master in Dinâmica dos Oceanos e da Terra, with emphasis in Geology and Geophysics.

Advisor: Prof. Dr. Antonio Fernando Menezes Freire
Co-advisor: Prof. Dr. Wagner Moreira Lupinacci

Niterói

2020

LAISA DA FONSECA AGUIAR

IDENTIFICATION OF BOTTOM SIMULATING REFLECTORS IN THE FOZ DO AMAZONAS BASIN, NORTHERN BRAZIL, USING SEISMIC AMPLITUDES, SEISMIC ATTRIBUTES AND FREQUENCY ANALYSIS

Dissertation submitted to the Programa de Pós-Graduação em Dinâmica dos Oceanos e da Terra of Universidade Federal Fluminense in partial fulfillment of the requirements for obtaining the degree of Master in Dinâmica dos Oceanos e da Terra, with emphasis in Geology and Geophysics.

Date: 14/02/2020

Examiners:

Dr. Antonio Fernando Menezes Freire – Universidade Federal Fluminense (Advisor)

Dr. Wagner Moreira Lupinacci – Universidade Federal Fluminense (Co-advisor)

Dr. Arthur Ayres Neto – Universidade Federal Fluminense

Dr. Roberto Salvador Francisco d'Ávila – PETROBRAS

DEDICATION

to my nieces Monalisa & Antonella,
thank you for bringing light and love to my journey.

ACKNOWLEDGEMENTS

Firstly, I want to thank my parents Sônia and Laumir for the unconditional love and support throughout this journey. I am also thankful for my grandma Dalva for the kindness, love and caring that she shares with me. Besides, I would like to thank my lovely sisters, Pâmella and Louise, for always taking care of me. I love you to the moon and back. Thank you for all the fish, you helped me to see with my eyes unclouded.

Second thanks go to Marvin, my *little bird*, for all the love, laughs, tears and understanding during this journey. Thank you for being my point of calm amid so many clouds. Let's fly together.

I would like to acknowledge my therapist, Junior, for all the help he provided in my searching for strength during this period of my life. I also want to acknowledge Pole&Art studio and all the wonderful, brilliant women I met there. Thank you for bringing joy to my life.

I would like to thank all my family and friends who have always been supportive of me. In special, I am so thankful for my lovely friends: Carol, Maíra and Yasmin, you made my life so much better in these two years, I could not be lucky enough. Thank you for everything.

Huge thanks to Eloíse and Ana Carolina, my "hydrate team", for all the joy and kindness that you bring to me. I am also thankful for Matheus Lima, Tone Rodrigues, Kenji Motoki, Danilo Ferreira and Flávio Oliver for the support you have given me. Your help made this dissertation possible.

I would like to thank my advisor, Dr. Fernando Freire, for all the guidance, patience, dedication and support through this dissertation. Thank you for encouraging me and believing in me in every step of this work. You are a great inspiration to me as a professional and as a human being. Once again, thank you for everything.

I would like to acknowledge the examiners of this dissertation, Dr. Arthur Ayres and Dr. Roberto D'Ávila for accepting evaluating this work. Thank you for your time and for contributing for this dissertation. I also would like to acknowledge Dr. João Marinho for reviewing this work. I am thankful for professor Dr. Wagner Lupinacci, my co-advisor, for his kindness and his suggestions on new approaches.

Finally, I am thankful for CAPES for the financial support for this dissertation; and to ANP for the permission to use the seismic of the Foz do Amazonas Basin from the database of Exploration and Production (BDEP).

“Drive away and try to keep smiling. Get a little rock and roll on the radio and go toward all the life there is with all the courage you can find and all the belief you can muster. Be true, be brave, stand.”

(Stephen King)

RESUMO

A Bacia da Foz do Amazonas é localizada na porção norte da Margem Equatorial Brasileira, ao longo da costa dos estados do Amapá e do Pará. A presença de hidratos de gás é sugerida nesta região em seções sísmicas de reflexão, através de refletores que simulam o fundo do mar (*Bottom Simulating Reflectors* - BSR). Este estudo pretende identificar feições sísmicas associadas aos hidratos de metano na Bacia da Foz do Amazonas através da interpretação sísmica, usando o *software* Petrel. Quatro seções sísmicas foram escolhidas para este estudo: 0239-0035, 0239-0034, 0239-0060-2-4 e 0270-2004b. Foram comparadas as amplitudes sísmicas do fundo do mar e do BSR em duas abordagens diferentes: manual e automática. Essas abordagens ajudaram a validar a feição sísmica inferida, já que os resultados mostraram uma inversão das polaridades no sinal entre o fundo do mar (positivo) e o BSR (negativo). Foram aplicados atributos sísmicos para reforçar esta visualização, tendo o atributo Envelope destacado o BSR na seção sísmica. Posteriormente, foi aplicada a decomposição espectral, que decompôs os dados sísmicos em quatro diferentes bandas de frequência: 10Hz, 20Hz, 30Hz, 40Hz, seguido novamente pela aplicação do atributo Envelope. Esta técnica permitiu melhorar a visualização do BSR e identificar intervalos em que este refletor anômalo é descontínuo. O uso integrado dessas abordagens validou a localização do BSR nas seções estudadas e permitiu inferir a ocorrência de hidratos de gás, revelando ser uma técnica útil para a interpretação da distribuição de hidratos de gás na Bacia da Foz do Amazonas, podendo ser utilizada em outras áreas.

Palavras-chave: Hidratos de Gás, Atributo Envelope, Amplitude Sísmica, Decomposição Espectral, Bacia da Foz do Amazonas.

ABSTRACT

The Foz do Amazonas Basin is located in the northern portion of the Brazilian Equatorial Margin, along the coast of the states of Amapá and Pará. The presence of gas hydrates is suggested in this region in reflection seismic sections, through reflectors that simulate the Bottom Simulating Reflectors - BSR. This study aims to identify seismic features associated with methane hydrates in the Foz do Amazonas Basin through seismic interpretation using Petrel software. Four seismic sections were chosen for this study: 0239-0035, 0239-0034, 0239-0060-2-4 and 0270-2004b. Seismic amplitude of the seabed and BSR were compared in two different approaches: manual and automatic. These approaches helped validate the inferred seismic feature, as the results showed a reversal of signal polarities between the seabed (positive) and the BSR (negative). Seismic attributes were applied to reinforce this view, with the Envelope attribute highlighted the BSR in the seismic section. Subsequently, spectral decomposition was applied, which decomposed the seismic data into four different frequency bands: 10Hz, 20Hz, 30Hz, 40Hz, followed again by the application of the Envelope attribute. This technique improved BSR visualization and identified intervals in which this anomalous reflector is discontinuous. The integrated use of these approaches validated the location of the BSR in the studied sections and allowed to infer the occurrence of gas hydrates, revealing to be a useful technique for the interpretation of gas hydrate distribution in the Foz do Amazonas Basin. It can be used in other areas.

Keywords: Gas Hydrates, Envelope Attribute, Seismic Amplitudes, Spectral Decomposition, Foz do Amazonas Basin.

LIST OF FIGURES

CONTENTS

1 PRESENTATION

This dissertation is written based on the results from the seismic interpretation of four 2D seismic sections of the Foz do Amazonas Basin, located at the northern portion of the Brazilian Equatorial Margin. By using the software Petrel, a comparison of seismic amplitudes between the seafloor and the seismic reflector of interest (Bottom Simulating Reflector - BSR) was executed, as well as application of seismic attributes and spectral decomposition.

The development of this dissertation complements the scientific article published in the journal Brazilian Journal of Geophysics, titled "ANALYSIS OF SEISMIC ATTRIBUTES TO RECOGNIZE BOTTOM SIMULATING REFLECTORS IN THE FOZ OF AMAZONAS BASIN, NORTHERN BRAZIL" (doi: http://dx.doi.org/10.22564/rbgf.v37i1.1988), which used only one seismic section (0239-0035). Methodology applied in the article consisted of the manual comparison between seismic amplitudes from the seafloor and the interpreted BSR, and the application of seismic attributes Envelope and Second Derivative of the Envelope.

For this dissertation, this methodology was expanded to other three seismic sections: 0239-0034, 0239-0060-2-4, 0270-2004b, where again manual comparison was made between seismic amplitudes and the application of the Envelope attribute. In addition, automatic extraction of seismic amplitude values was performed, which allowed the comparison between manual and automatic approaches. A frequency spectrum analysis was also executed, enabling the application of the Spectral Decomposition attribute together with the Envelope, in order to enhance the recognition of the BSR and its lateral continuity.

1.1 Dissertation structure

This dissertation is organized in a total of **8 chapters**: The first three chapters are this presentation, introduction, containing the main goals for this research, and geologic settings of the Foz do Amazonas Basin. The fourth chapter presents a literature review, briefly describing relevant aspects of methane hydrates and seismic attributes; the fifth chapter addresses the methods used in this work, the sixth presents the discussion of the

results, and finally in the seventh chapter the conclusions obtained are reviewed. The last chapter contains all the references used for this work.

2 INTRODUCTION

The Foz do Amazonas Basin has been the target of several studies concerning its geologic settings, gravitational tectonics, gas hydrates distribution, and the occurrence of hydrocarbons. The evolution of the basin is related to the formation of the Central Atlantic Ocean and its sedimentation extends from the continental margin to the deep-sea fan of the Amazonas River (Soares et al., 2008).

The occurrence of natural gas hydrates on continental margins worldwide, including the Foz do Amazonas Basin, is of increasing interest as a result of its energy potential (Kvendolven, 1993; Sloan Jr, 2003; Joshi et al., 2017). There are other significant environmental aspects related to methane hydrates that are noteworthy, such as their consequences on the planet's climate, as an enhancer of the greenhouse effect, and in the context of instability of the seafloor (Kvendolven, 1993), which according to several authors can trigger mass movements (Flood & Piper, 1997; Maslin & Mikkelsen, 1997; Piper et al., 1997; Maslin et al., 2005). These aspects stimulate research strategies in this scientific area (Aguiar et al., 2019).

The presence of methane hydrates can be inferred from Bottom Simulating Reflectors (BSR) on seismic reflection data. A BSR is a seismic reflector parallel to the seafloor that coincides with the base of the Gas Hydrate Stability Zone (GHSZ), characterized by a negative reflectivity, i.e. polarity opposite to the seafloor (Hyndman & Spence, 1992; Kvendolven, 1993). The BSR is inferred to coincide with the phase boundary, and separate solid hydrates above from free gas below (Kvendolven, 1993). Thus, these well-marked reflection works as a seismic signature to identify and map gas hydrates (Joshi et al., 2017).

Seismic attributes are excellent tools for seismic interpretation and are progressively relevant for the exploration of hydrocarbons (Taner et al., 1994). The development of seismic attributes is connected to advances in computational. According to Taner et al. (1994) and Taner (2001), attributes were introduced in the early 1970s, where they were initially used only as a visualization tool. This perspective quickly evolved to their use in the qualitative interpretation of geometry and physical subsurface parameters. More recently, with the calibration of seismic data with well data, the use of

attributes has sought a more quantitative approach in order to infer seismic characteristics.

The use of seismic attributes allows the extraction of information concerning subsurface geometry and physical parameters to obtain detailed knowledge about the geological context of a prospect (Taner et al., 1979). The choice of an attribute depends on the specific reservoir environments, the mathematical foundation of the attribute and what is this attribute sensitive to (Chen & Sidney, 1997).

Spectral decomposition is a technique that has been widely used in the exploration industry, since it contributes to optimize reservoir characterization. By interpreting in frequency domain, it might be possible to extract interesting information from seismic data, such as thin-bed interference, geologic discontinuities and identification of anomalies related to the accumulation of hydrocarbons (Partyka et al., 1999, Oliveira, 2009; Oliveira et al., 2010).

As stated in Aguiar et al. (2019), there are considerable studies that applies seismic attributes in order to examine and investigate the presence of gas hydrates in different regions around the world (Coren et al., 2001; Satyavani et al., 2008; Ojha &Sain, 2009; Oliveira, 2009; Oliveira et al., 2010; Canario, 2013). The use of attributes can allow the identification of BSR and its continuity (Coren et al., 2001), and help inferring patterns related to the occurrence of gas hydrates and free gas below the Gas Hydrate Stability Zone (Satyavani et al., 2008).

This study aims to propose effective ways to identify the presence of BSRs in the Foz do Amazonas Basin. In this work, the software Petrel was used for the interpretation of 2D reflection seismic data obtained from the Exploration and Production Database (BDEP) of the Brazilian National Agency of Petroleum, Natural Gas and Biofuels (ANP – Agência Nacional do Petróleo, Gás Natural e Biocombustíveis).

2.1 Objectives

The main goal of this dissertation is to find techniques that recognize Bottom Simulating Reflectors (BSR) associated to the possible occurrence of methane hydrates in the Foz do Amazonas Basin. Through seismic interpretation and therefore the identification of these reflectors, it will be possible to infer potential gas hydrates occurrences in this region. Below, specific objectives taken for this research are listed.

i. identifying and interpreting the seafloor and the Bottom Simulating Reflector (BSR) in four distinct seismic sections: 0239-0035, 0239-0034, 0239-0060-2-4 e 0270-2004b;

ii. comparing seismic amplitudes between seafloor and possible BSR in these four lines in order to validate the inferred seismic feature in two distinct approaches (manual and automatized);

iii. to apply several seismic attributes using the software Petrel, then choosing the ones that best highlighted the BSR;

iv. to analyze the frequency spectral cases and therefore to apply the spectral decomposition attribute;

v. to interpret the seismic sections with spectral decomposition along with the Envelope applied.

3 GEOLOGIC SETTING

The study area of this dissertation is the Foz do Amazonas Basin. This basin is located in the northern portion of the Brazilian Equatorial Margin and occupies a total area of approximately 268,000 km^2. It is situated along the coastal zone of Amapa and in part of northwest coast of Para state (Brandão; Feijó, 1994); (Figueiredo et al., 2007). Figure 1 shows location map of the seismic survey with the four seismic lines used for this work.

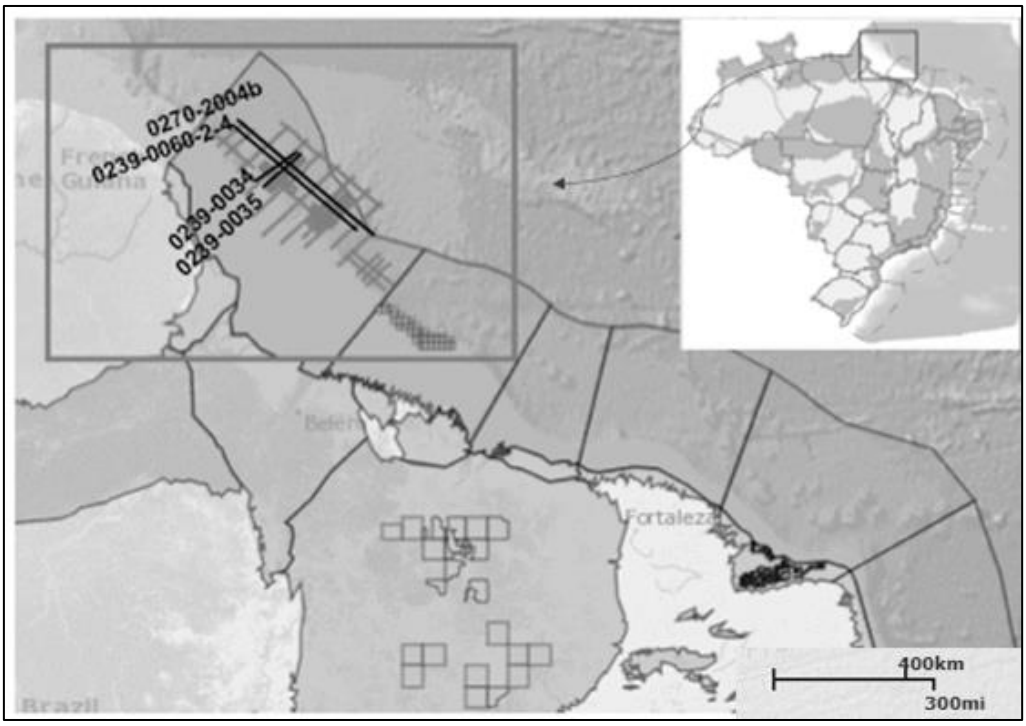

Figure 1: Location map of the seismic survey provided by the Exploration and Production Database (BDEP) for the Foz do Amazonas Basin. Source: http://webmaps.anp.gov.br/mapas/Lists/DSPAppPages/MapasBrasil.aspx;

The sedimentation area of Foz do Amazonas basin includes the continental shelf, the slope and the deep-water region, also known as Amazon River Cone (Soares et al., 2008). According to Bruno (1987), 55% of the area occupied by this basin corresponds to the continental shelf, which extends to the bathymetric level of -200m, whereas 45% corresponds to the deep-water region.

As stated by Damuth & Kumar (1975), the Amazon River Cone (or Submarine Fan of the Amazon River) can be considered one of the largest deep submarine cones in the world, and its sedimentation is provided mainly from the Amazon River. The

Submarine Fan of the Amazon River is the morphological feature of greatest expression in the Foz do Amazonas Basin (Araújo et al., 2009).

In the following topics, it is addressed the geological context in which Foz do Amazonas basin is inserted, in addition to some aspects from the tectono-sedimentary evolution of this basin.

3.1 Geological context of Foz do Amazonas Basin

The tectonic evolution of the Foz do Amazonas Basin is associated with the rupture of the supercontinent Gondwana, during the Aptian, that caused the separation of South American and African tectonic plates and the consequent formation of the Atlantic Ocean (Carvalho, 2008). Similarly, the structural configuration from this basin follows the one in the Delta do Níger basin, located at the west African margin (Pasley et al., 2004; Carvalho, 2008).

The process of evolution of the basins of the Brazilian Equatorial Margin, including the Foz do Amazonas Basin, can be divided in 4 stages of deformation, as follows: 1) extension NE-SW, during the Triassic-Jurassic; 2) E-W extension in the Neocomian; 3) two phases of dextral shear during the Aptian-Cenomanian, forming the "Dextral Transtractional Corridor", extending from the Foz do Amazonas Basin to the Potiguar Basin, and 4) oceanic scattering during the Late Cretaceous to the Cenozoic (Azevedo, 1991; Carvalho, 2008).

According to Soares et al. (2008), the structural framework of the Foz do Amazonas Basin can be explained through three tectonic events. The first event occurred in the Late Triassic and was associated with the formation of the Central Atlantic Ocean, which formed an elongated hemigraben limited by normal direction faults (NW-SE), whose magmatism culminated in the formation of the volcanic rocks of the Calçoene Formation; the second tectonic event was in the Early Cretaceous and formed an elongated graben that contains sediments of the Cassiporé Formation. Finally, the third tectonic event began in the Albian and is linked to the final process of separation of the African and South American plates, resulting in formation of the passive margin and the onset of transform faulting in an ENE-WSW direction that segmented the margin.

The sedimentary filling of Foz do Amazonas basin is composed by two stratigraphic sequences of the rift and passive margin phases. Thus, the rift phase is characterized by Cassiporé Formation (inferior to Cenomanian) and Calçoene (inferior to Jurassic). Passive margin section can be subdivided into two intervals: pre-Amazon (Cenomanian to middle Miocene) and Amazon-fan (late Miocene to Recent) (Pasley et al., 2004; Soares et al., 2008).

3.1.1 Amazon River Cone

The Amazon River Cone, as stated before, corresponds to the morphological feature of greatest expression in the Foz do Amazonas Basin (Araújo et al., 2009), whose formation is associated to a high rate of siliciclastic sedimentation input to the Atlantic Ocean, since the middle Miocene, as a result of the uplift of the Andes Mountain Chain (Rimington *et al*., 2000; Figueiredo *et al.*, 2007; Pasley et al., 2004).

The Amazon Fan deposition is related to the Andean Orogeny that caused the inversion of the Amazon River (Carvalho, 2008), transforming the Amazon River into a major drainage system during the late Miocene (Rimington *et al*., 2000; Pasley et al., 2004).

The Submarine Fan of the Amazon extends about 700 km from the continental shelf break (Rimington et al., 2000) and reaches bathymetric depths up to 4800 m, with a gradient of 0.4° (Rimington et al., 2000; Da Silva, 2008; Araújo et al., 2009). Cobbold *et al*. (2004) estimated that the cone has a thickness of approximately 10 km, with an average sedimentation rate of 1m/ka.

The Amazon fan is a depocenter in which its loading drives gravitational collapses (Reis et al., 2010, 2016; Ketzer et al., 2018). Several authors point to the existence of Mass Transport Deposits - MTD linked to gravitational landslides in the central region of the Amazon Cone, and the dissociation of methane hydrates could be a possible trigger for these landslides (Piper et al., 1997; Araújo et al., 2009).

Damuth & Kumar (1975) delimited the Amazon Cone in three compartments according to changes in its gradient: upper (up to -3000 m of bathymetric level), middle (up to -4200m) and lower (up to -4800 m). The upper slope concentrates huge mass-

transport deposits (MTD) that depict the Neogene stratigraphic succession of the fan (Reis et al., 2010, 2016; Silva et al., 2016; Ketzer et al., 2018). Therefore, the focus of this dissertation is concentrated on the Neogene where it hosts the upper slope gas hydrate system (Aguiar et al., 2019).

The recent work published by Ketzer et al. (2018) investigates gas seepage from the Gas Hydrate Stability Zone (GHSZ) on the Amazon Fan. In this study, they were able to gather evidence that about 60% of gas vents are located along seafloor faults that register undergoing gravitational collapses of the fan, whereas 40% are in water depths of 650m-715m within the upper edge of GHSZ. This could suggest the role of fluid migration along pathways created by faulting in this region (Ketzer et al., 2018).

The presence of gas hydrates within the Amazon deep-sea fan has been inferred from BSR through several studies (Manley and Flood 1988; Sad et al., 1998; Tanaka et al. 2003; Berryman et al. 2015 *apud* Ketzer et al., 2018), and recently confirmed by seafloor sampling of fluid seeps.

4 LITERATURE REVIEW

4.1 Gas hydrates definition

Gas hydrates are naturally occurring solids that are formed from a combination between water and gas (mainly methane) (Kvenvolden, 1998). They occur under proper conditions of temperature, pressure and composition, within the Gas Hydrate Stability Zone – GHSZ (Kvenvolden, 1998; Sloan, 2003). These substances resemble ice or compressed snow (Figure 2) and are stable when the constituents come into contact under low temperature and moderate pressure (Sloan, 2003).

Gas hydrates are formed when small guest gas molecules (such as methane or carbon dioxide), in contact with water at appropriate temperature (typically less than 300 K) and pressure (usually greater than 0.6MPa) are encaged (enclathrated) by crystalized water cavities (Sloan, 2003). This causes the gas molecule to be trapped within this structure and, for this reason, these solids are also known as clathrates (Freire, 2010).

Figure 2: Gas hydrates and their resemblance with snow. Retrieved from Freire (2010).

As reported by Sloan (2003), there are three gas hydrates structures: cubic structure I, which predominates in the Earth's natural environments and contains small gas molecules; cubic structure II, which hosts relatively larger guests in mostly artificial environments; and hexagonal structure H that might occur in both environments, but only with a mixture of small and large gas molecules. Additionally, gas hydrates may be considerable simple if formed by only one gas molecule for each cage; double, with more

than one gaseous component, separated by a cavity; and mixed, if formed by more than one gas molecule in the same cavity.

4.2 Gas hydrates formation

Methane contained in gas hydrates may be thermogenic or biogenic in origin. Thermogenic origin is linked to the thermal transformation of organic matter at great depths, where temperatures can reach values above 60 °C, while the biogenic origin of methane is associated with the deterioration of organic matter by decomposing microorganisms, usually at temperatures below 60°C (Paull et al., 1994 apud Clennell, 2000). Therefore, it is irrefutable that organic matter content is essential to gas hydrates formation. Thus, biogenic clathrates are not common in abyssal zones or in regions with low rate of sedimentation (Paull et al., 1994 apud Clennell, 2000), except for hydrates related to thermogenic gas exudations. In recent studies of Ketzer et al. (2018), the molecular of gas trapped in hydrates in sediments of the Amazon fan are consistent with a biogenic origin, whereas those on the adjacent continental slope area are related to a possible thermogenic contribution to the gas mix.

According to Kvenvolden (1993), gas hydrates occur worldwide, but due to pressure/temperature and gas volume requirements, their formation are limited to two regions: polar and deep oceanic. In polar regions, gas clathrates are associated with permafrost environments. In deep oceanic regions, gas hydrates are found in outer continental margins, in adjacent continental slope area.

Gas Hydrate Stability Zone can be defined in terms of temperature and pressure, although there are other factors that contribute for clathrate formation in natural environments, such as thermodynamic conditions, geothermal variation in stability zone, degree of saturation and salinity and water temperature. Besides, gas composition, conditions of porosity/permeability and physico-chemical parameters of sediments which host hydrates are also aspects that influence clathrates occurrence and stability (Kvenvolden, 1993). Figure 3 illustrates a hydrate stability zone for marine environments.

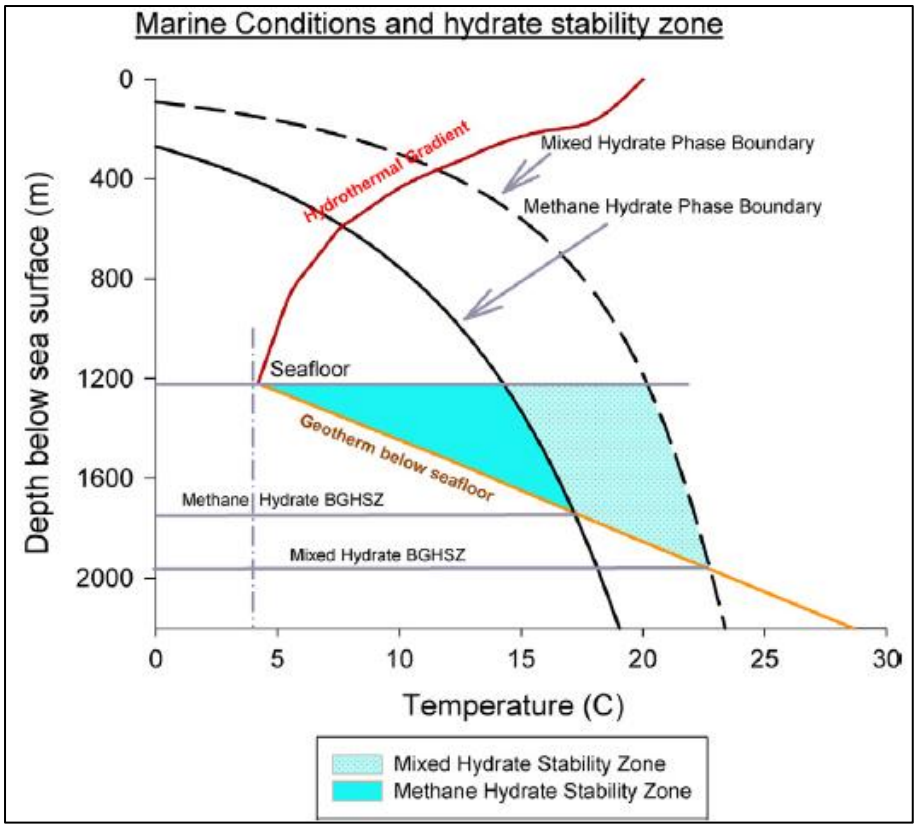

Figure 3: An illustration of a gas hydrate stability zone for marine environment. Source: Chong et al., 2016.

4.3 Recognition of gas hydrates

The identification and characterization of methane hydrates can be done through geochemical studies, direct methods (cores and dredges) or indirect (seismic, echosounder, well logs and geoelectric methods) (Freire, 2010; Miller et al., 2015). Other indirect ways of identifying gas hydrates, associated with natural gas seeps or mud volcanoes, are realized through high-resolution imaging of the seafloor using Remoted Operated Vehicle (ROV) (Freire, 2010).

In general, the seismic reflection method is the most indirect method used to infer the presence of methane hydrates, through the identification of an anomalous bottom simulating reflection (BSR) that may be associated with blanking (reduction in reflection amplitude), as well as seafloor mounds or pockmarks (Shipley et al, 1979; Kvenvolden, 1993; Katzman et al., 1994; Gehrmann et al., 2009 apud Miller et al., 2015; Freire et al., 2011).

In seismic profiles, blanking corresponds to a seismic feature that occurs due to the presence of gases, leading to a decrease in acoustic impedance contrasts, which results

in a reduction of the amplitudes of seismic reflections (Lee et al., 1993 apud Rosa et al., 2006).

Pockmarks are features identified in seismic sections that can be associated with gas seepages processes that may occur due to the dissociation of methane hydrates. These processes happen through fault zones and fractures, forming chimney features that can be extended from the reservoir to the seabed (Hovland & Judd, 1988 apud Rosa et al., 2006; Clennel, 2000).

The presence of gas hydrates is often inferred from Bottom Simulating Reflectors, which delineate the maximum depth of the gas hydrate stability zone (Kvenvolden, 1993; Lorenson & Kvenvolden, 2001). These anomalous reflectors are characterized by reflection polarity opposite to the seafloor (Kvenvolden, 1993; Hyndman & Spence, 1992).

In summary, Bottom Simulating Reflector corresponds to a seismic reflector that is parallel to the seafloor and is generally characterized by reflection polarity reversals (reflections opposite to those from seafloor) (Kvenvolden, 1993). BSRs mark the acoustic impedance contrast between gas hydrate stability zone (higher sonic velocity, hydrate-cemented sediment) above and lower sonic velocity, possibly containing free gas below the layer of stability zone. This interface between higher-velocity strata overlying lower-velocity strata generates a reflector with negative polarity in relation to the seafloor coefficients (Kvenvolden, 1993; Singh *et al*., 1993 apud Freire, 2013; McConnell & Kendall, 2002). Figures 4 and 5 illustrate how BSR can be identified in a seismic section.

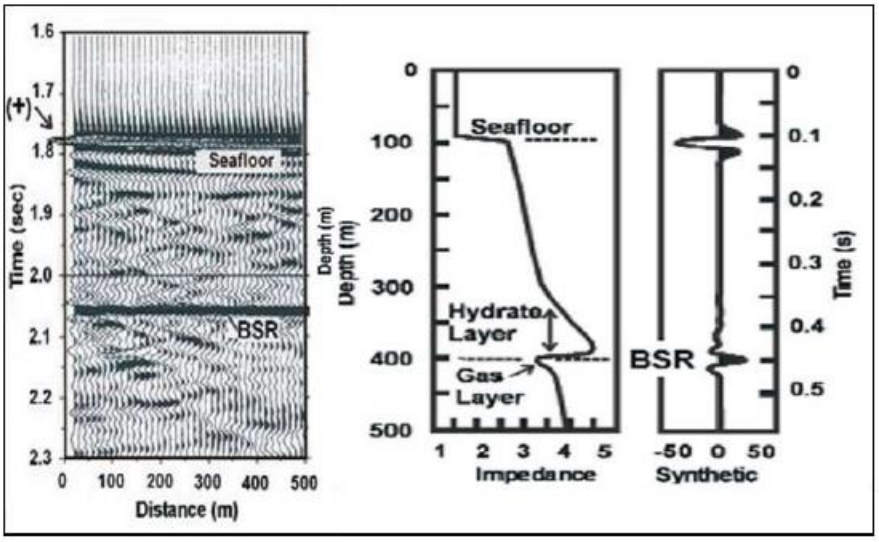

Figure 4: A schematic of how a BSR can be identified in a seismic section. BSR has an inverted polarity in relation to the seafloor. Source: Freire, 2017.

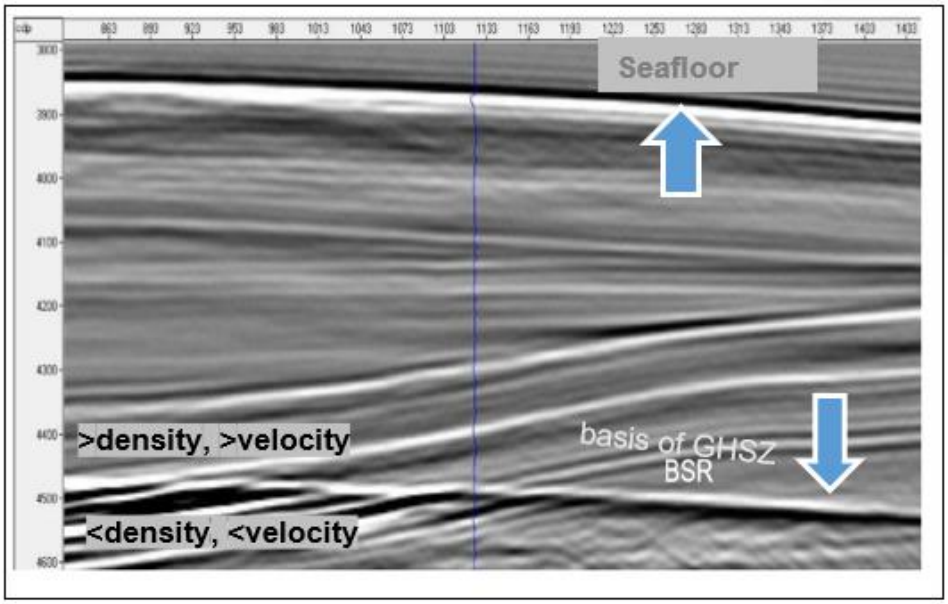

Figure 5: BSR identified in a seismic section. Modified from Pintas (2011).

4.3 Seismic attributes definition

Taner (2001) and Taner et al. (1994) defined seismic attributes as information that can be acquired from seismic data, either by direct/statistical measurements or by the interpreters' experience. By applying these attributes, it is possible to obtain new notions and a more detailed and precise knowledge of the structural, stratigraphic and lithological characteristics of a given seismic prospect (Taner et al., 1979).

The choice of attributes depends on the nature of each and the circumstances in which they might be useful, so that a given attribute may be more sensitive to certain reservoir environments, while some are better at revealing underground anomalies or as indicators of hydrocarbons (Chen & Sidney, 1997).

Taner et al. (1979) have developed a mathematical foundation for attribute computing, where the amplitude of these seismic trait is treated as the real part of a complex analytic signal, while the imaginary part is extracted through the Hilbert Transform (Chopra & Marfurt, 2005). Combination of the incoming seismic trait with the Hilbert Transform results in the so-called Instant Attributes, which are computed sample by sample and represent the instantaneous variation of several parameters. They are: Envelope, instantaneous phase, instantaneous frequency, Envelope derivatives, among others (Taner et al., 1979; Taner, 2001; Russel, 2004).

Taner et al. (1979) observed that, from the analysis of the seismic signal as an analytical signal (i.e, analysis of the complex seismic trace), it is possible to separate the two components of the seismic trace, amplitude and phase. The amplitude of the seismic data is considered as the main factor for the determination of physical parameters, such as acoustic impedance, reflection coefficients, velocities and absorption. The phase component is the main factor in determining the shapes of the reflectors and their geometric configurations (Taner, 2001).

4.3.1 Seismic attributes classification

Several authors have contributed to the classification of seismic attributes in different groups. This work will follow the classification proposed by Taner in the official publication of the 2001 Canadian Society of Exploration Geophysics (CSEG). Firstly, the attributes are classified as Pre-Stack or Post-Stack, based on the characteristic domain of each attribute. They can also be classified according to their computational characteristics (Aguiar et al., 2019). In the following topics, there is a briefly explanation of the main classification of attributes used in this study.

Post-Stack attributes

During the stacking process, azimuth and offset information are lost. The input data is stacked or migrated CDPs. Migration in time maintains the relations of time and temporal variables as the frequency has its dimension preserved. For sections migrated in depth, the frequency is replaced by the wave number. This type of attribute is best suited for analyzing large volumes of data in initial studies (Taner, 2001).

Attributes related to geology

In this context, attributes can be divided into physical and geometric categories. Physical attributes are commonly used for lithologic classification and reservoir characterization, relating subsurface parameters to lithological characteristics (Taner, 2001), whereas geometric attributes are used for stratigraphic and structural interpretation. In this work, after attempts to select the best attributes to emphasize the BSR of the analyzed seismic section, one physical attribute presented fine results: the Envelope, since it strengthen the signal amplitude. The next topic describes this attribute and its main characteristics.

4.3.2 Envelope

The Envelope attribute is also known as "instantaneous amplitude", "Envelope amplitude" or "reflection strength" (Taner et al., 1979; Chen & Sidney, 1997). The theoretical basis of the instantaneous attributes was developed by (Taner et al., 1979) and it is based on the analysis of the complex seismic trace:

$$C(t) = s(t)+ih(t) \qquad (1)$$

where s(t) corresponds to the real part of the complex seismic trace; h(t) is the Hilbert Transform of the seismic trace, the imaginary part of the trace (also known as quadrature - Russell, 2004). The imaginary component h(t) is obtained by applying the Hilbert Transform in the seismic trace s(t), under the following conditions for h(t):

1. It is determined from s(t) by a linear convolution operation;
2. Reduce to the phasor representation (in complex numbers) if s(t) is a sinusoidal function.

If these conditions are met it is possible to determine h(t) for any s(t) that can be represented by a Fourier series or integral (Taner et al., 1979). The use of the complex seismic trace allows computing instantaneous amplitude, instantaneous phase and instantaneous frequency in simple harmonic oscillation logic extensions. Therefore, the complex seismic trace can be rewritten in polar form:

$$C(t) = A(t)e^{i\theta(t)} \qquad (2)$$

where A(t) is the envelope of the seismic trace (or amplitude/instantaneous energy) and corresponds to the complex function module C(t):

$$A(t) = \sqrt{s(t)^2 + h(t)^2} \qquad (3)$$

The Envelope is phase independent and is sensitive to changes in acoustic impedance, emphasizing changes in amplitude of the original seismic section. This attribute is related to reflectivity because it is proportional to the acoustic impedance contrast. In addition, it can be a good discriminant of numerous geological features, such as bright spots,

possible gas accumulations, unconformities, changes in lithology and deposition environments, sequence limits, among others (Taner, 1992, 2001).

4.4 Spectral Decomposition

Spectral Decomposition decomposes seismic data into the frequency domain (Partyka et al., 1999). This technique is widely used for reservoir characterization and in exploration industry, since it can be used as a Direct Hydrocarbon Indication (DHI), as well as a tool for mapping bedding thickness and geologic discontinuities (Partyka et al., 1999; Castagna et al., 2003; Oliveira, 2009; Oliveira et al., 2010).

According to Partyka et al. (1999), frequency domain in general is usually more interesting because it allows interpreters to identify thin-bed interference, and therefore to find textures and patterns related to geologic processes, which may not be visible in original seismic sections (Oliveira, 2009). These features can also be represented by sub bands of frequency.

Time-frequency representation can be computed by different methods, such as Short-Time Fourier Transforms (STFT), Continuous Wavelet Transform (CWT), S Transform (ST), among others (Oliveira, 2009). The choice between these methods depends on the application, its parameters and the expected results, additionally to understanding the advantages and disadvantages of each method.

Computing Spectral Decomposition helps delineate stratigraphic settings, such as channel sands and faults systems (Partyka et al., 1999), as this time-frequency decomposition turns an 1D trace signal into a 2D signal of time and frequency, and describes how the spectral content of the signal changes with time (Liu et al., 2011).

One of the most used methods for time-frequency analysis is Short-Time Fourier Transform, where it produces a spectrum by taking a Fourier transform in a time window that moves along with the signal. Since the results will be based on length and kind of window used, this method leads to a compromise between temporal and spectral decomposition (Oliveira, 2009; Liu et al., 2011).

As stated in Oliveira et al. (2010), in order to apply spectral decomposition in a seismic section, it is essential to decompose each seismic trace, followed by adjusting the data into common frequency groups, also known as isofrequency panels. Then, for

interpreting this data, the interpreter must analyze the isofrequency panels for finding geological features that result in anomalous spectral amplitudes.

The context behind the application of spectral decomposition consists of the nature of seismic wave propagation, since while it propagates, it loses energy due to spherical divergence, scattering, intrinsic absorption and reflection (Tai et al., 2009). Therefore, the responses for the reflected seismic wave in amplitude and frequency depends on different factors.

Tai et al. (2009) listed these factors as geologic structure, bedding thickness, lithology, pore fluid properties, source wavelet. Additionally, when a seismic wave returns to the surface, it also brings information related to stratigraphic features and hydrocarbon accumulation, in a way that each reservoir has its own seismic frequency response due to its rock/fluid properties. Hence, using spectral decomposition might be useful for extracting characteristic frequency components from seismic data, aiding imaging and mapping of bed thickness, discontinuities, identification of low frequency anomalies associated to hydrocarbons and attenuation (Partyka et al., 1999; Castagna et al., 2003; Tai et al., 2009).

There are only a few reported works that uses spectral decomposition in order to characterize gas hydrates systems (Stein et al., 2007 apud Oliveira et al., 2010), such as studies from reserves located in Japan (Hato et al., 2006). In Brazil, most researches that applies time-frequency analyzes are from methane hydrates reserves in Pelotas Basin, located in the south of Brazilian Continental Margin (Oliveira, 2009; Oliveira et al., 2010).

5 METHODS

5.1 Seismic data input and quality control

The first step in this work was the loading of seismic data in time, provided by the National Agency of Petroleum (ANP) – Exploration and Production Database (BDEP), into the software Petrel. Initially, the coordinates of the study region for the creation of the "Foz do Amazonas" project were defined. After the establishment area covered by the seismic survey, 70 seismic lines of 2D reflection were imported.

Due to the large number of seismic lines, a sorting was carried out to choose the most appropriate seismic profiles for the execution of this study. Seismic profiles were previously interpreted by the author of this dissertation to analyze their quality and to extract preliminary knowledge about the main seismic reflectors. Thus, lines 0239-0035, 0239-0034, 0239-0060-2-4 and 0270-2004b were selected because they present interesting features, possibly related to gas hydrates. Figures 6, 7, 8 and 9 show these sections with no interpretation.

5.2 Comparing amplitudes and applying seismic attributes

In this step, one graph for each seismic section was created to analyze the behavior of seismic amplitudes from the mapped BSR in comparison to the seafloor, in order to assure the BSR location in the seismic. For sections 0239-0035, 0239-0034, and 0270-2004b the BSR were also divided in two distinct sectors (sector 1 and sector 2). This division was made in order to ease seismic interpretation.

This step was taken in two different approaches: manual and automatic. During the manual procedure, the values of seismic amplitudes from the seafloor and the BSR were taken by passing the cursor exactly on the trace number and time of the reflector of interest, especially whenever there was a strongest reflection. However, these values were determined in variable intervals of trace number, i.e., for seismic section 0239-0035 for every 2 trace number interval, a value was noted; although for the other three seismic lines (0239-0034, 0239-0060-2-4, and 0270-2004b) for every 5 trace number interval, a value was noted.

Throughout the automatic approach, it was used a Petrel tool named surface attribute. Then, an “Extract Value” attribute was applied for each interpreted horizon, and thereafter a spreadsheet was generated in order to produce graphs for each seismic section. During this procedure, for every trace number a value from the seismic amplitude was taken.

Subsequently, some seismic attributes were applied to highlight the identified BSR in the four sections and, therefore, to infer the base of the Gas Hydrate Stability Zone (BGHSZ). The Envelope attribute was the seismic attribute chosen that best enhanced the BSR, after several attempts.

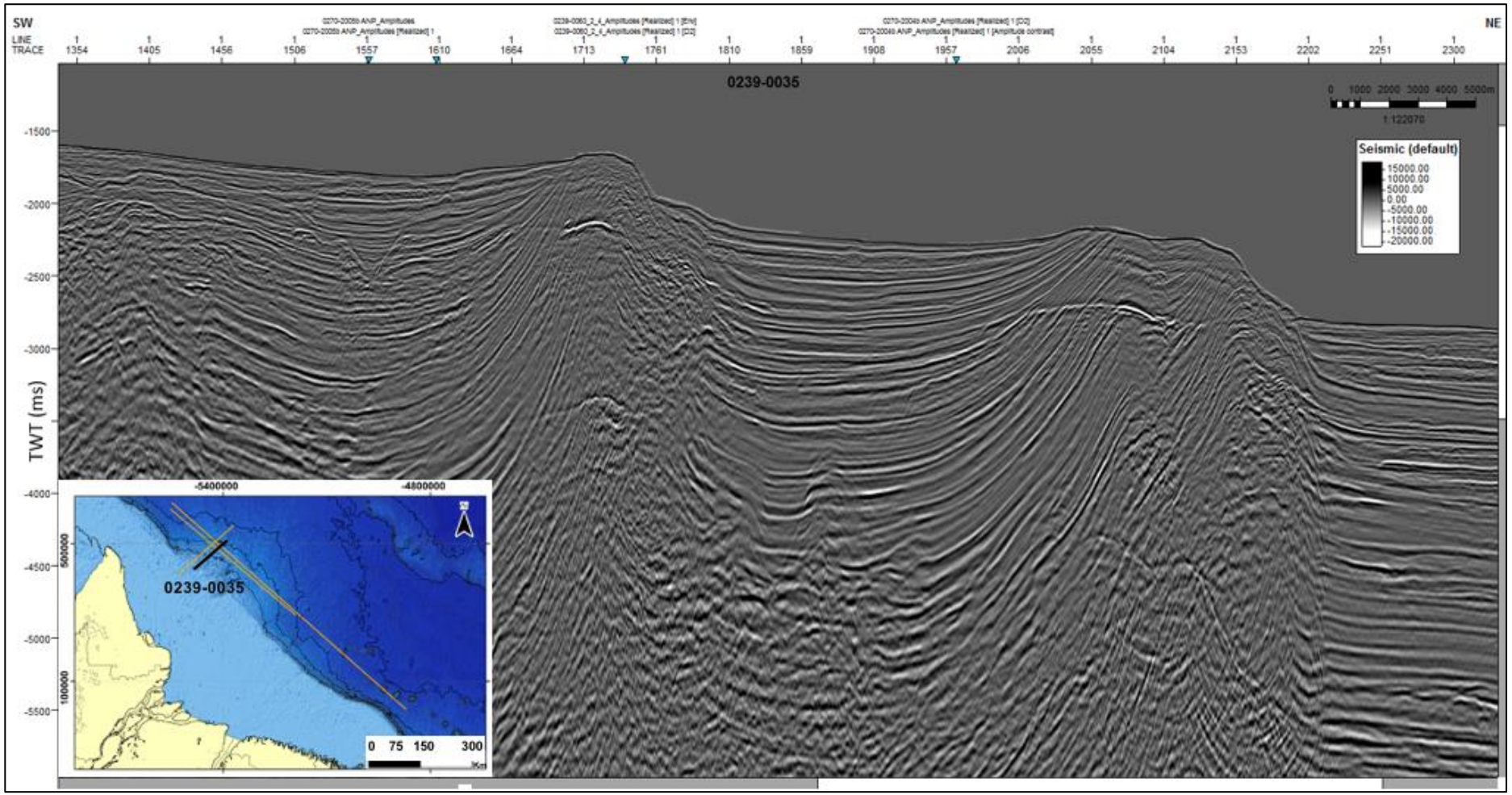

Figure 6: Seismic section 0239-0035 with no interpretation. Location of this line is highlighted in black.

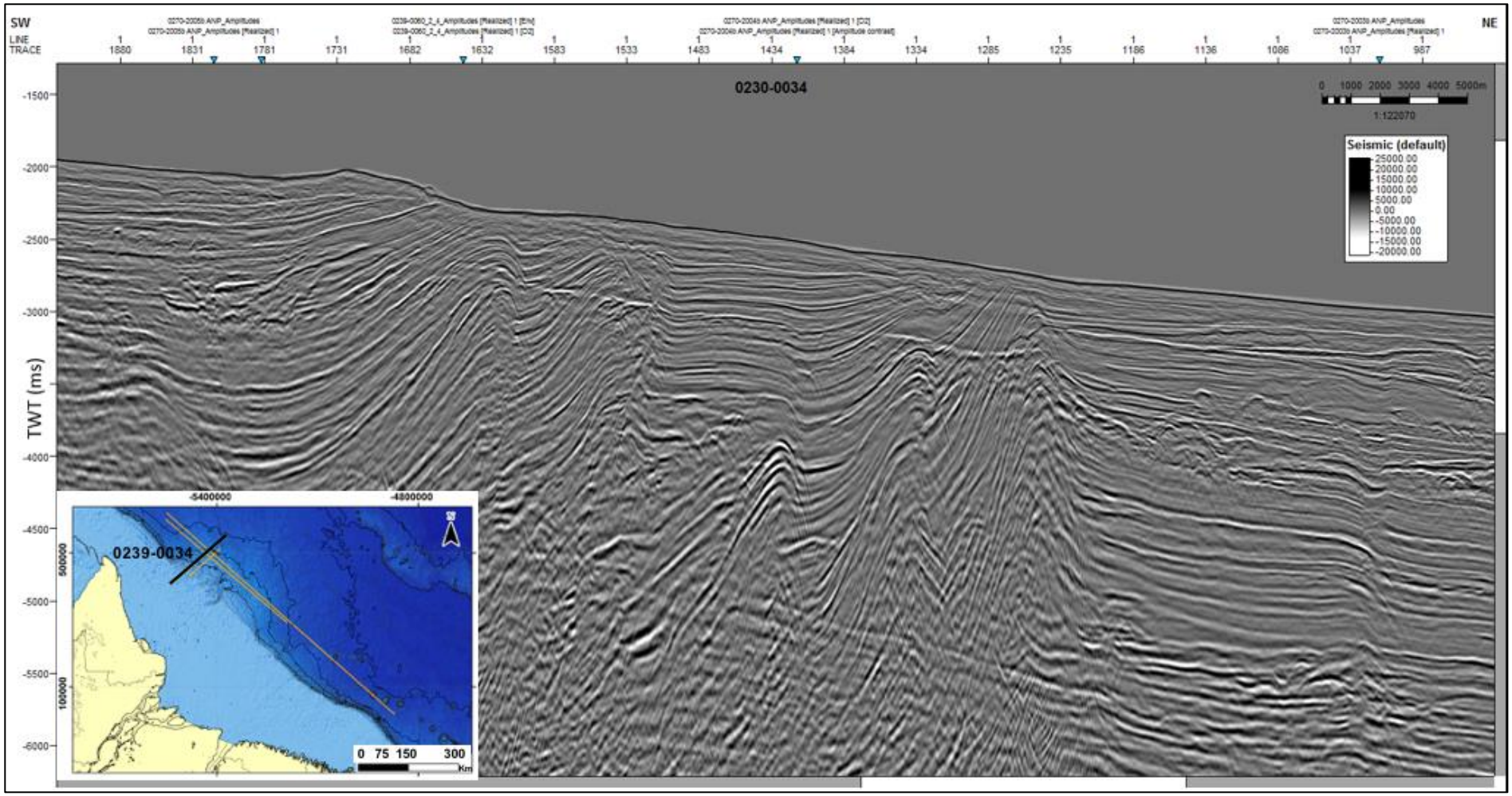

Figure 7: Seismic section 0239-0034 with no interpretation. Location of this line is highlighted in black.

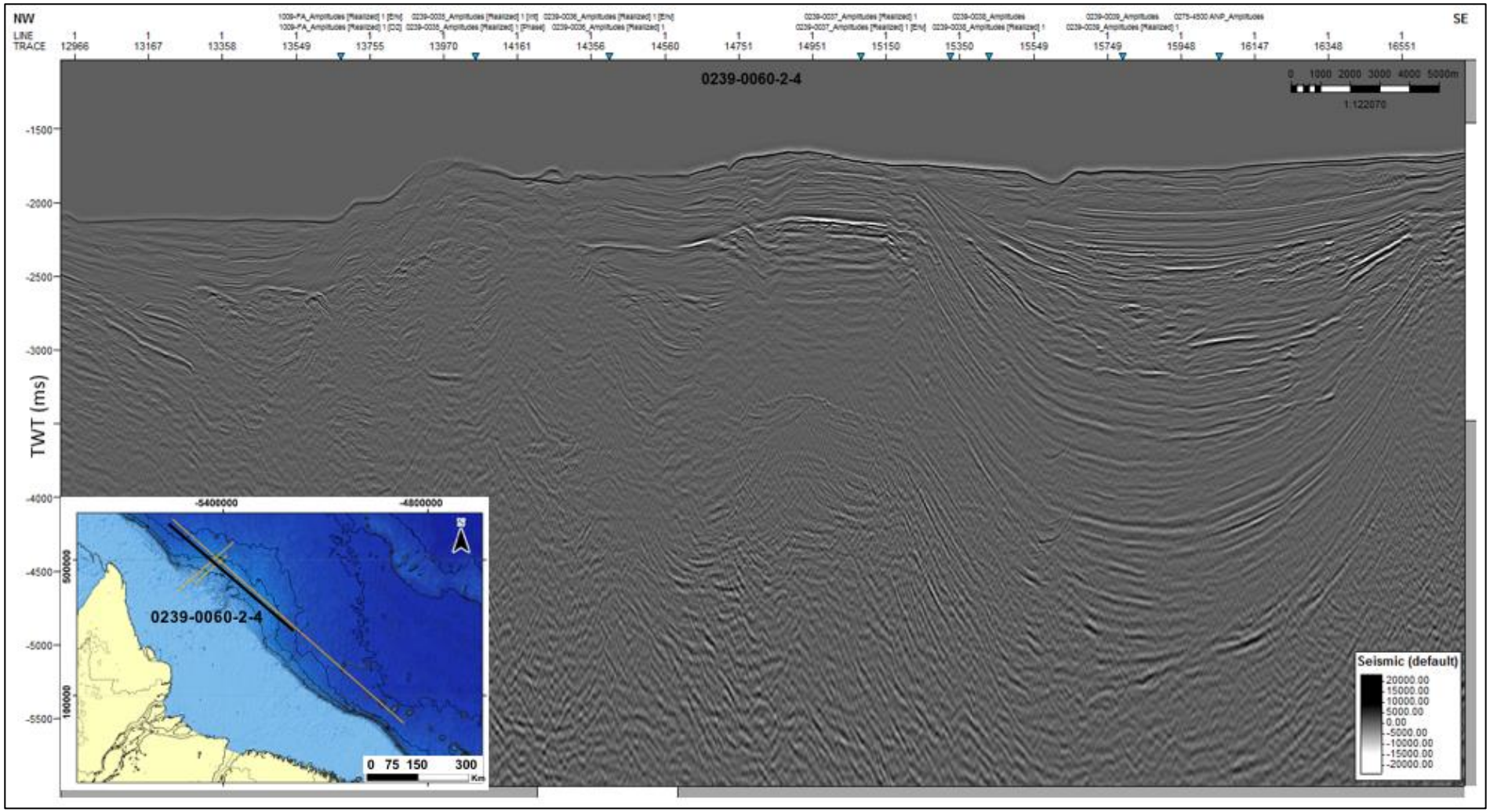

Figure 8: Seismic section 0239-0060-2-4 with no interpretation. Location of this line is highlighted in black.

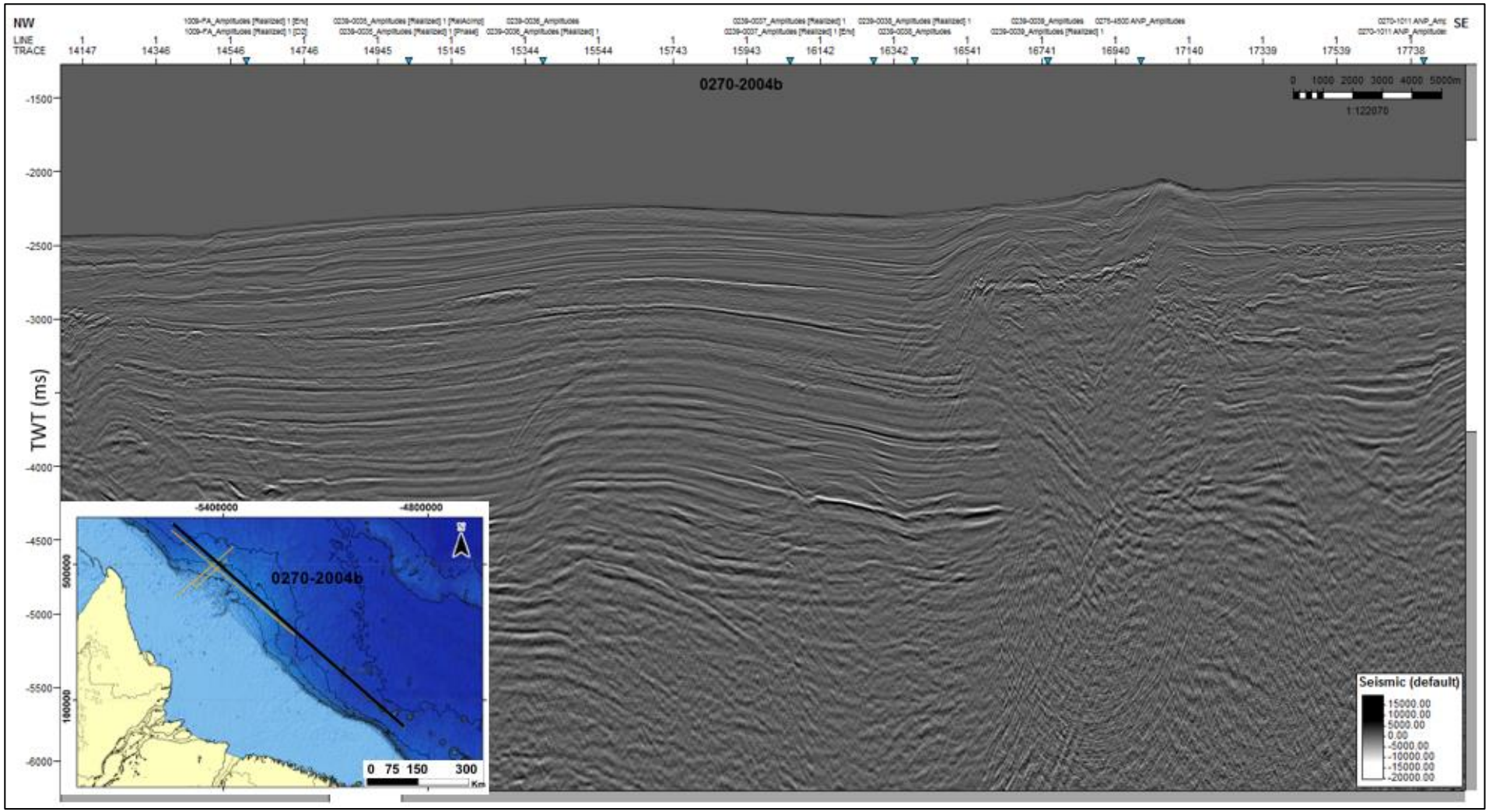

Figure 9: Seismic section 0270-2004b with no interpretation. Location of this line is highlighted in black.

5.3 Applying Spectral Decomposition

Firstly, in order to apply the attribute Generalized Spectral Decomposition (GSD) correctly, it was necessary to evaluate the frequency spectral for the four seismic lines. Since the main goal of this dissertation is to attempt different ways for recognizing Bottom Simulating Reflectors, a virtual cropping of the sections was executed, in a way that only those frequencies who best contribute for the BSR and therefore within potential methane hydrates reserves were selected.

After analyzing the frequency spectral using the frequency spectral cases tool on Petrel, four frequency bands were established to implement GSD attribute: 10Hz, 20Hz, 30Hz, and 40Hz. Before applying GSD in each seismic line, a few parameters were defined as the default suggested by Petrel, such as algorithm (convolution), phase (90º) and number of cycles (2.0).

Subsequently to decomposition of the seismic data into four frequency bands as mentioned above, Envelope attribute was calculated for each band in order to enhance visualization of the BSR.

6 RESULTS AND DISCUSSIONS

6.1 Seismic interpretation

Through the methodology described above, it was possible to interpret seismic sections 0239-0035, 0239-0034, 0239-0060-2-4 and 0270-2004b, and to identify negative amplitude reflections interpreted as BSR (white lines), an indicative of the existence of methane hydrates in the Foz do Amazonas Basin. The following Figures 10, 11, 12 and 13 present these seismic sections interpreted. This initial interpretation corresponds to the basis of this work, and the following steps will either validate or discard what is proposed in this section.

When a BSR crosscuts strata reflections that are not parallel to the seafloor, it is sharp and easily identified. In sections where the stratification is parallel to the seafloor, BSR can be harder to identify (Freire et al., 2011; Holbrook et al., 2002). Therefore, interpreting BSR based on the non-conformity of this reflector in contrast with seismic reflectors representing the bedding is a very useful primary approach for identifying BSR.

The analysis of seismic amplitude and the use of seismic attributes can help mitigate uncertainties in BSR recognition, in the interest of inferring the presence of gas hydrates (Aguiar et al., 2019). For this project, sections 0239-0035, 0239-0034 and 0270-2004b were analyzed in two sectors (named sector 1 and sector 2). This division in sectors was made so that seismic interpretation turns out easily. Besides, for lines 0239-0035 (Figure 10) and 0270-2004b (Figure 13), there is an interval of uncertainty that is highlighted.

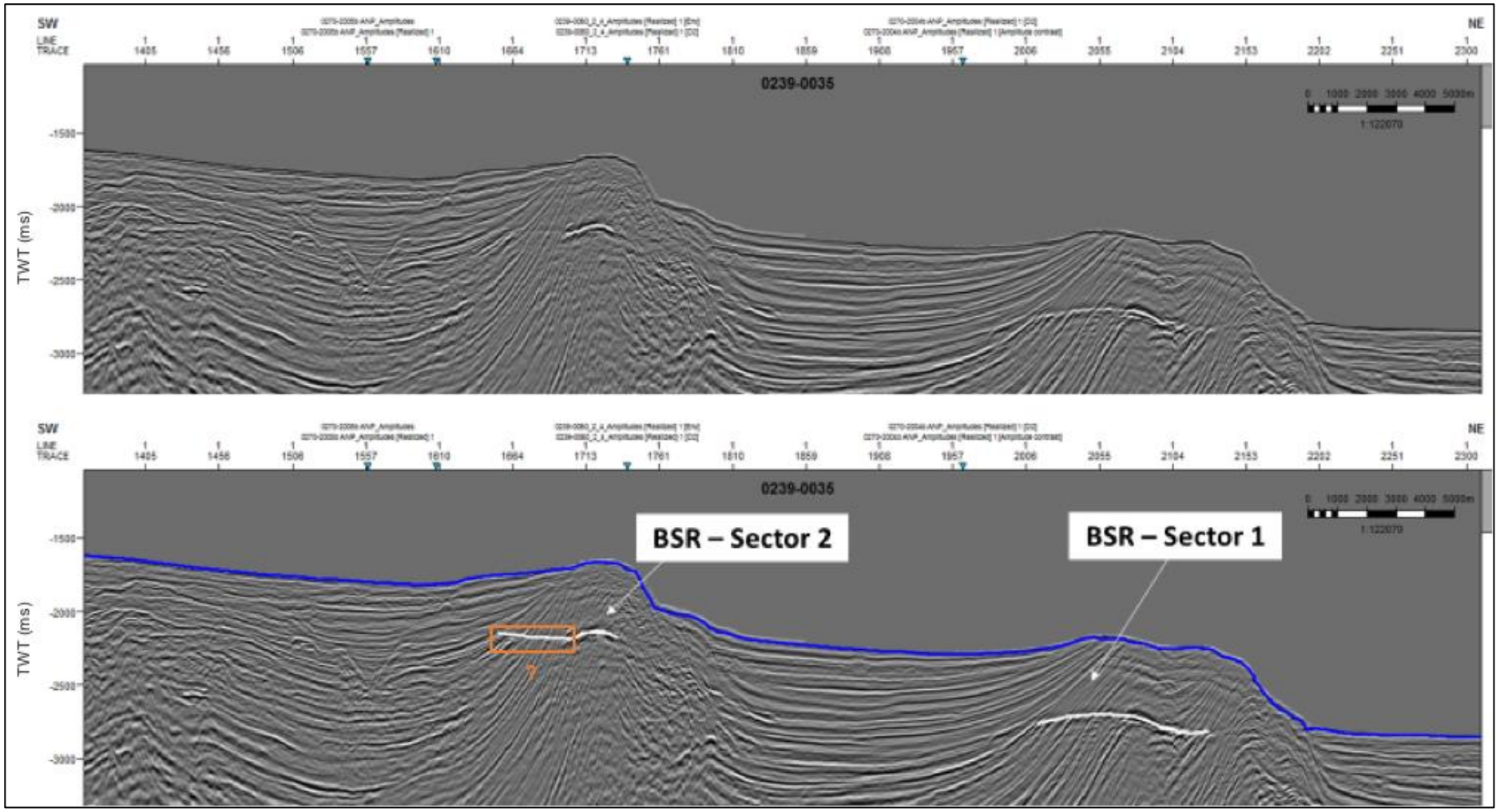

Figure 10: Seismic line 0239-0035 with no interpretation (top) and with the two sectors of BSR horizon (white lines) (bottom). Highlighted in orange, there's an interval of greater uncertainty for interpretation, which might imply that BSR is weaker or simply does not exist.

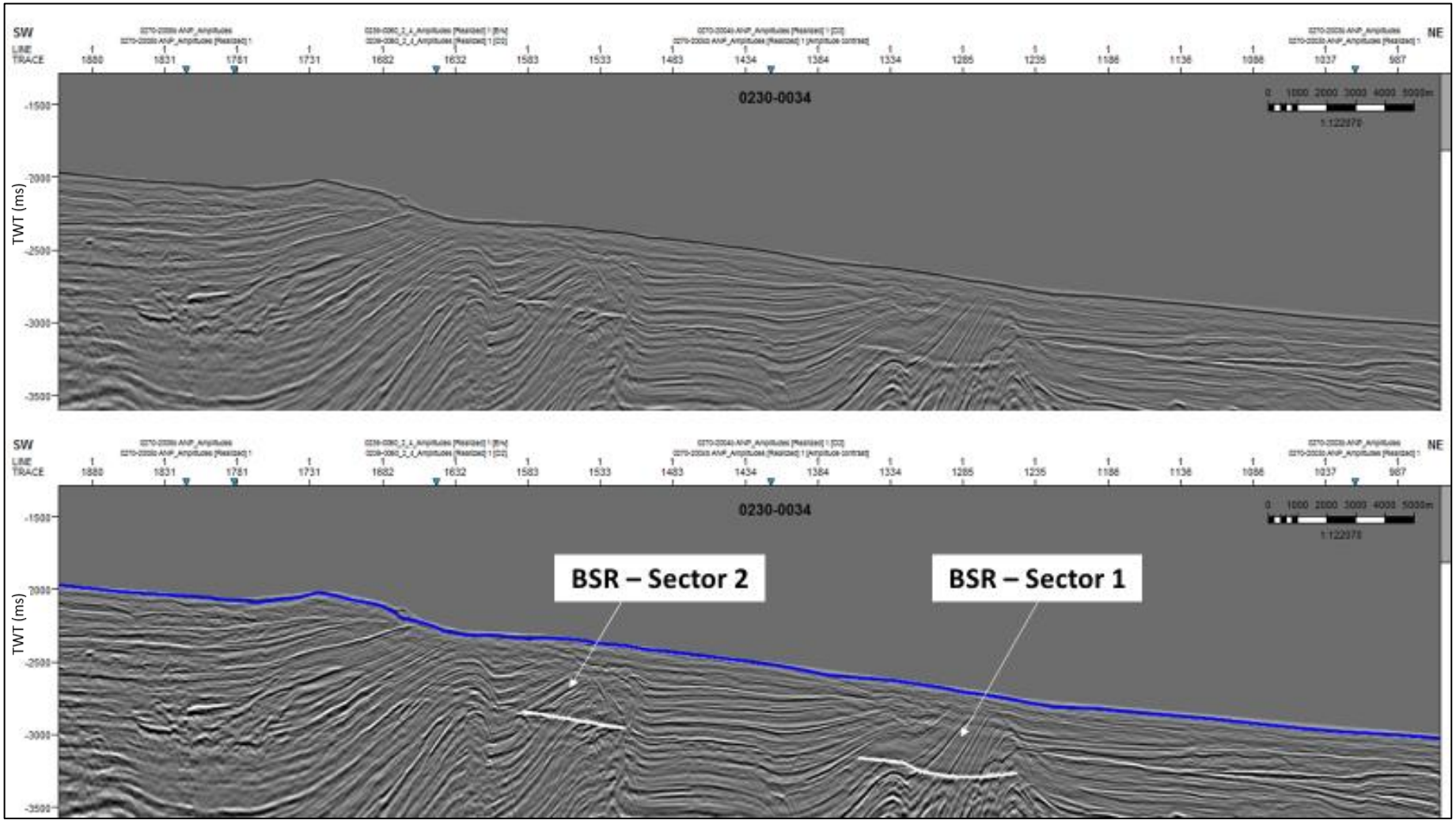

Figure 11: Seismic line 0239-0034 with no interpretation (top) and with the two sectors of BSR (white lines).

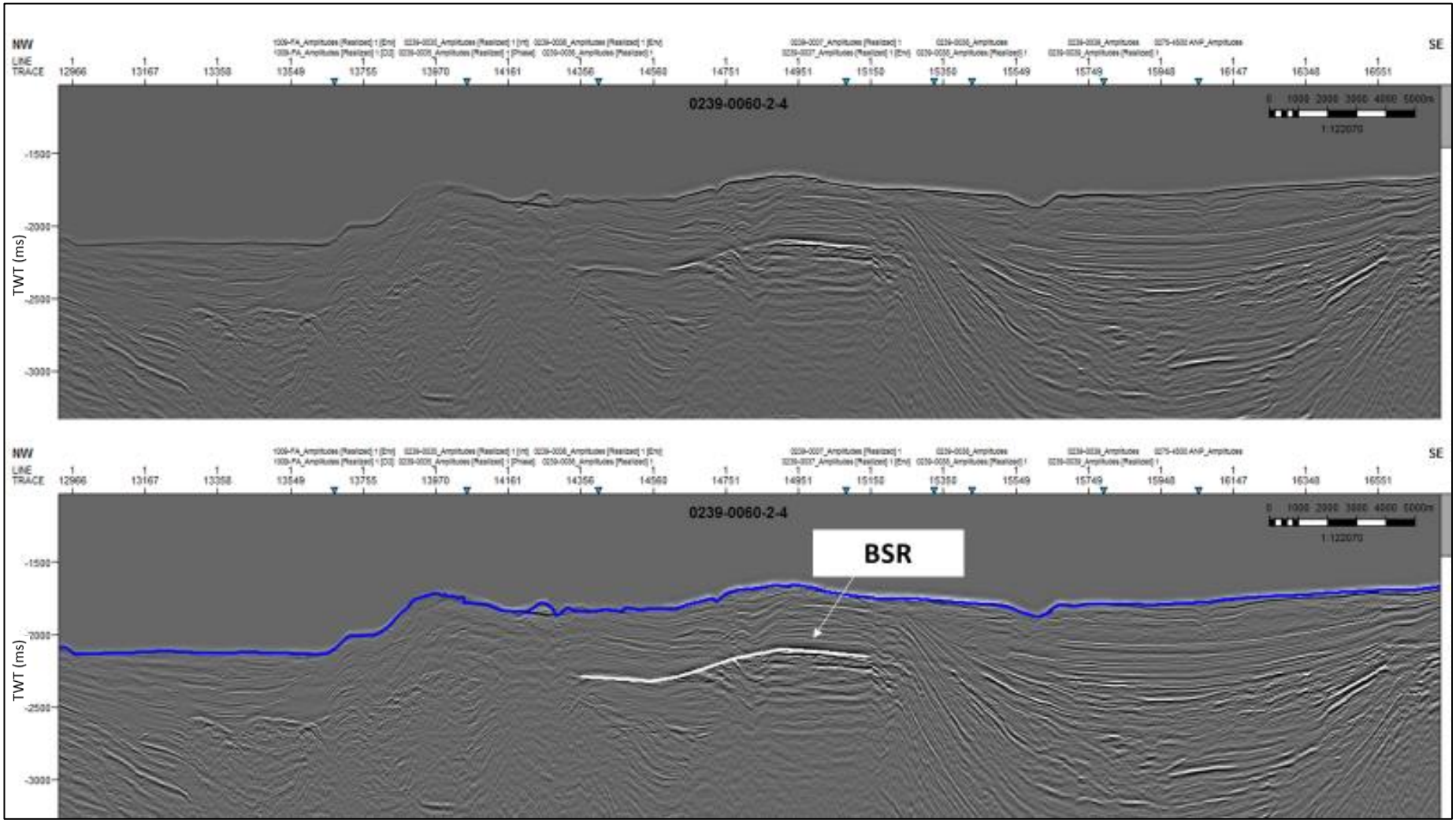

Figure 12: Seismic line 0239-0060-2-4 with no interpretation (top) and with the BSR interpreted (white line).

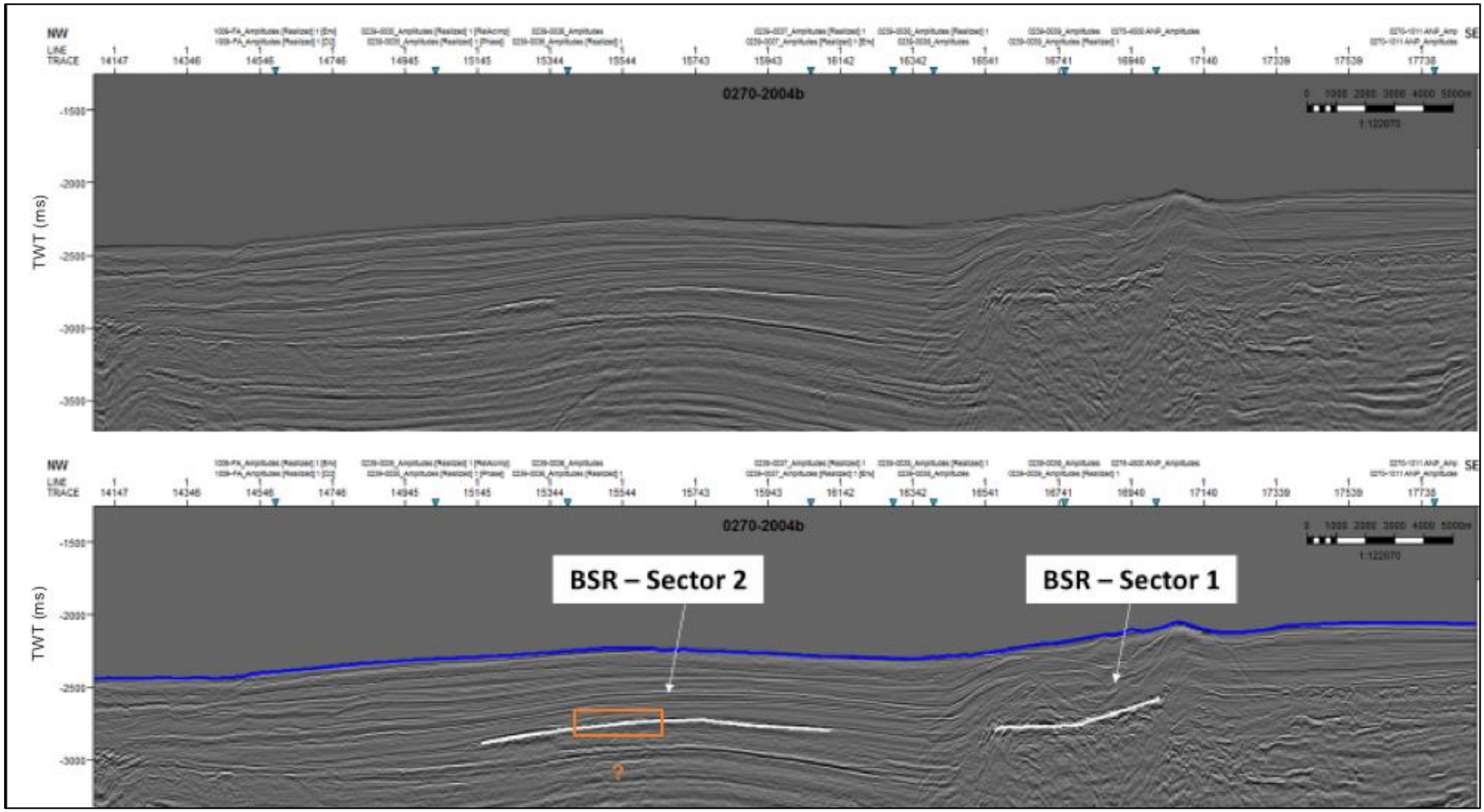

Figure 13: Seismic line 0270-2004b with no interpretation (top) and with the two sectors of BSR (white lines). Highlighted in orange, there's an interval of greater uncertainty for interpretation, which might imply that BSR is weaker or simply does not exist.

6.2 Comparison of seismic amplitudes of the seafloor and the BSR

According to Kvendolven (1993), the seismic reflector that coincides with the lower limit of the gas hydrate stability zone can be defined by reversed polarity, in comparison to the seafloor coefficients. Theoretically, the amplitudes of well-marked BSRs are expected to be negative and large (Dillon et al., 1996; Aguiar et al., 2019)

In order to validate the location of the BSR and infer the presence of methane hydrates associated to these features, it is compared the seismic amplitudes for the two sectors of BSR in sections 0239-0035, 0239-0034, 0270-2004b, and in section 0239-0060-2-4, in which these seismic reflectors can be observed. This comparison between seismic amplitudes was executed by using two different approaches: manual and automatic.

Appendix shows the tables that contains the results based on the **manual** picking of the seismic amplitudes, i.e, when the amplitudes were taken by passing the cursor exactly on the trace number and time of the reflector of interest.

Through the “Extract Value” surface attribute on Petrel, where it was applied for each interpreted horizon, it was possible to extract seismic amplitudes from the seafloor and the BSR, in order to produce graphs for each seismic section. Since during this procedure for every trace number a value from the seismic amplitude is computed, there is simply an enormous amount of data. Therefore, tables containing all the amplitude data obtained through the automatized approach will not be shown in this dissertation.

The graphs for the amplitude data picked **manually** and **automatic** for the four seismic sections are plotted in the Figures 14 to 20 for seismic sections 0239-0035, 0239-0034, 0239-0060-2-4 and 0270-2004b, respectively.

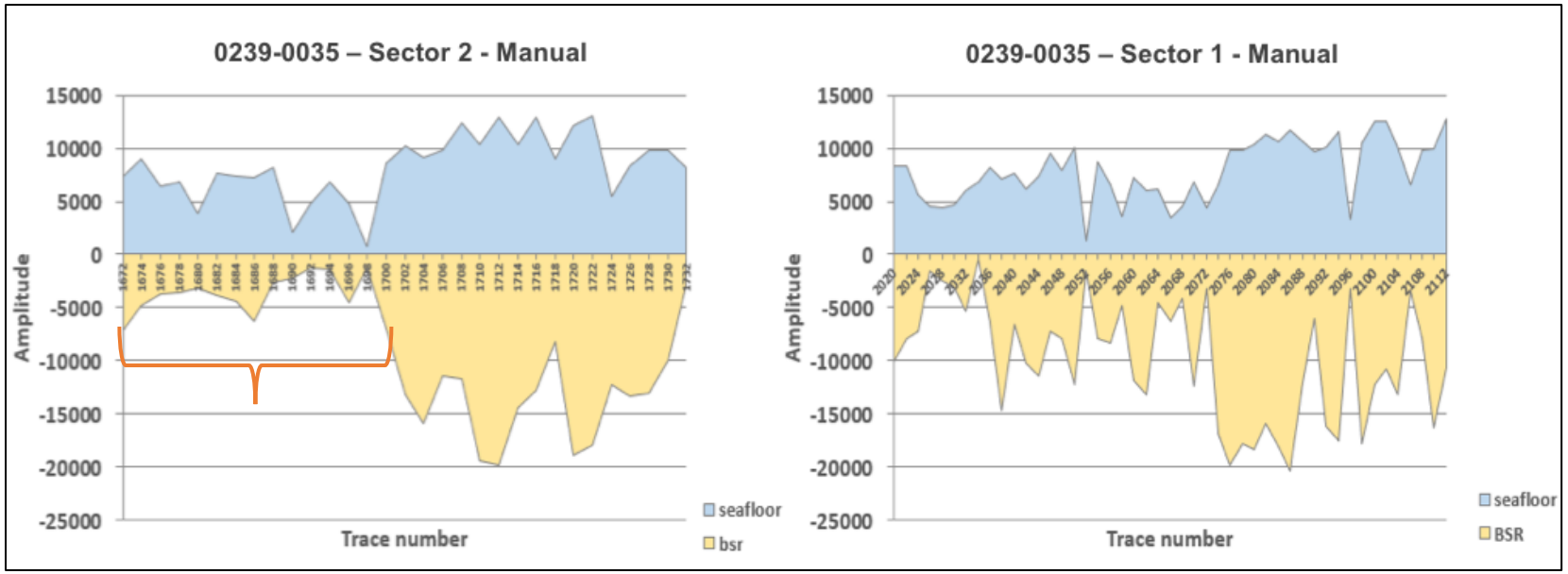

Figure 14: Seismic amplitudes of section 0239-0035 on the seafloor and the BSR - sector 1 and sector 2 (manual). An inversion in polarity between the seafloor (positive) and the BSR (negative) can be observed. Highlighted in orange, it is possible to notice the interval of uncertainty in sector 2, where values of BSR amplitudes are too small to be considered BSR.

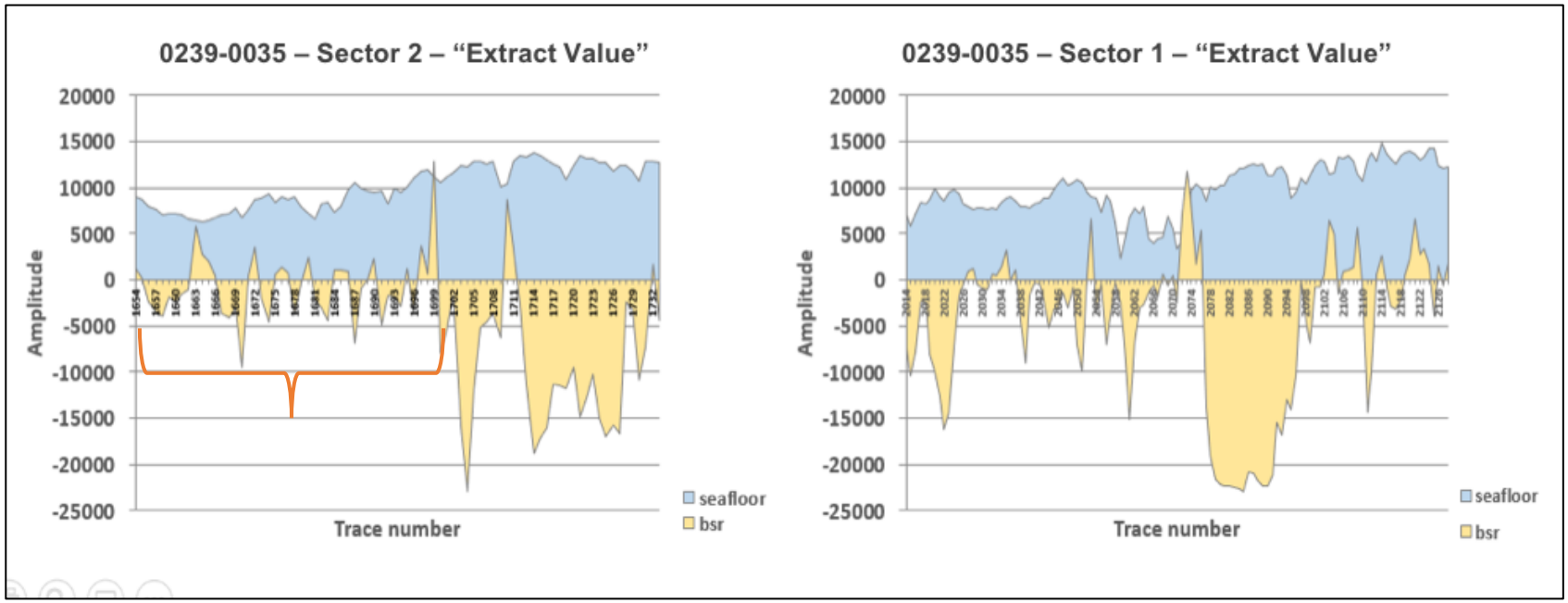

Figure 15: Seismic amplitudes of section 0239-0035 on the seafloor and the BSR - sector 1 and sector 2 (using attribute Extract value). An inversion in polarity between the seafloor and the BSR is noticed in both sectors, although this inversion is not always continuous. Highlighted in orange in sector 2, once again it is possible to observe the interval of uncertainty, where most values of BSR amplitudes are positive, which suggests the non-existence of BSR in this interval.

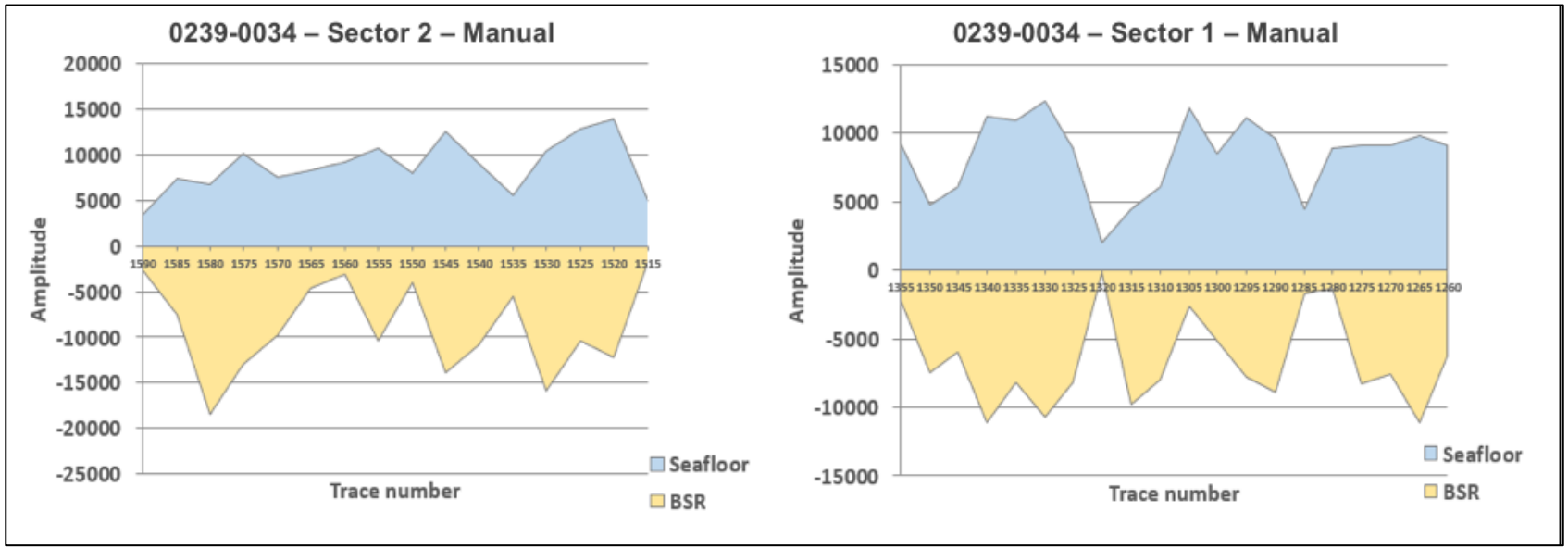

Figure 16: Seismic amplitudes of section 0239-0034 on the seafloor and the BSR - sector 1 and sector 2 (manual). It is possible to notice an inversion in polarity between seafloor (positive) and BSR (negative). However, these graphs present very sharp behavior, which could be explained by the small amount of data obtained from the manual picking interval (every 5 trace number).

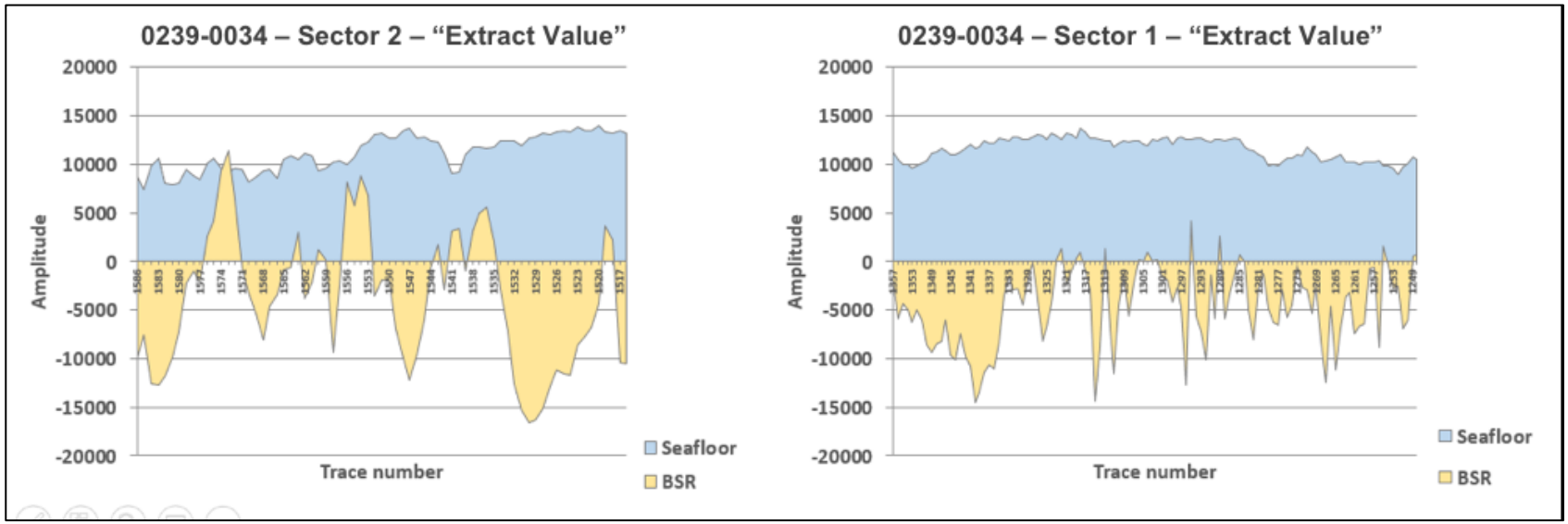

Figure 17: Seismic amplitudes of section 0239-0034 on the seafloor and the BSR - sector 1 and sector 2 (using attribute Extract Value). These graphs are smoother than the ones obtained using manual approach. There is an inversion in polarities between seafloor and BSR, although this inversion is not continuous, which suggests a lateral discontinuity of BSR.

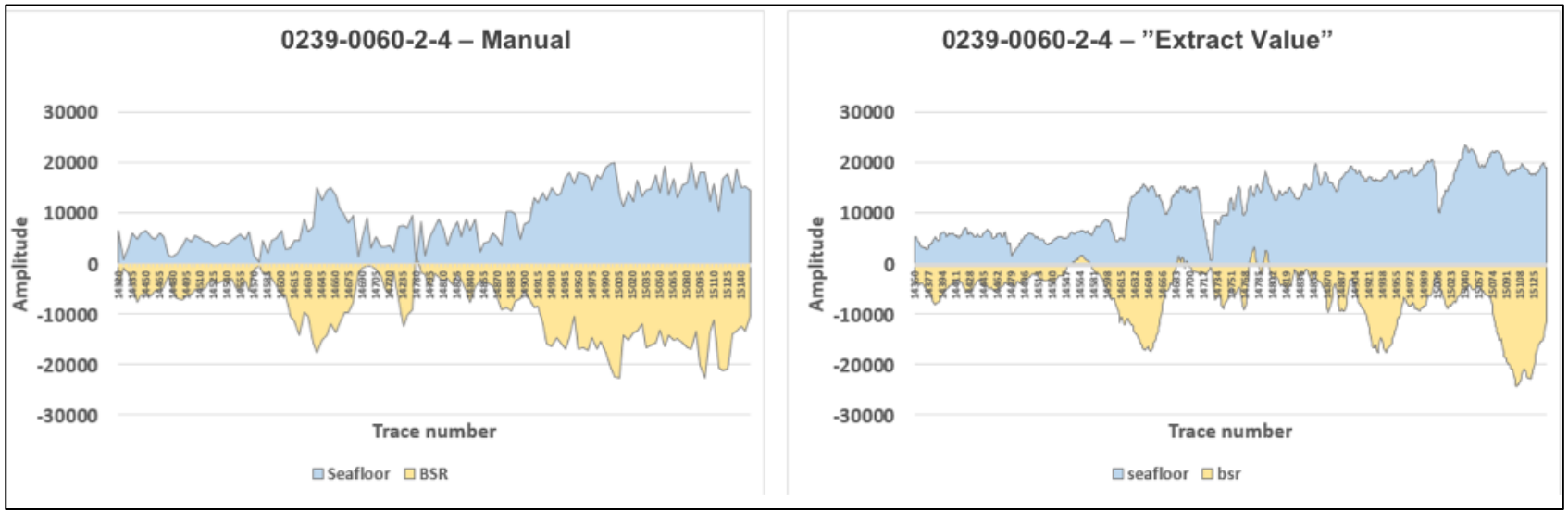

Figure 18: Seismic amplitudes of section 0239-0060-2-4 on the seafloor and the BSR obtained through manual (left) and automatized (right) approaches. It is evident in these graphs the inversion in polarity between the seafloor (positive) and the BSR (negative). Also, they present very similar behaviors for the comparison of seismic amplitudes.

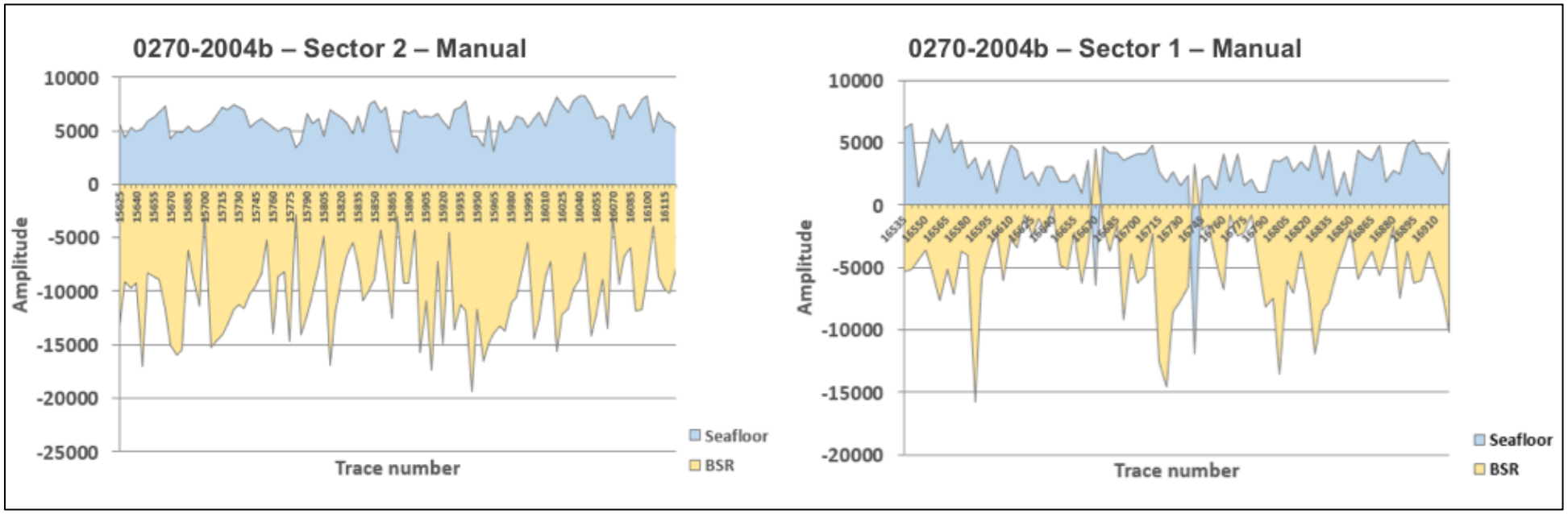

Figure 19: Seismic amplitudes of section 0270-2004b on the seafloor and the BSR - sector 1 and sector 2 (manual). The inversion in polarities between seafloor and BSR is noticed, and it is possible to point out negative and large values of BSR, as expected in theory. However, positive values for BSR are also observed, suggesting the non-continuity of BSR.

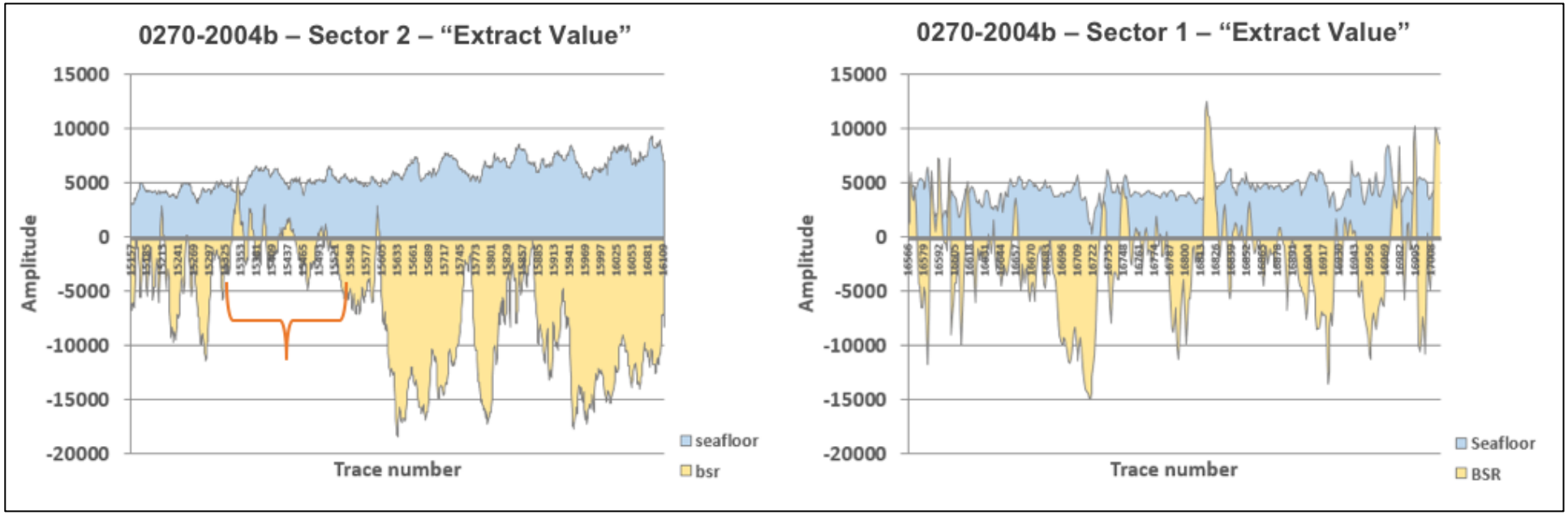

Figure 20: Seismic amplitudes of section 0270-2004b on the seafloor and the BSR - sector 1 and sector 2 (using attribute Extract Value). These graphs present similar behavior to the ones obtained using manual approach. It is possible to notice intervals where BSR values are negative and large. However, there are portions where BSR showed positive values, implying BSR discontinuity. Highlighted in orange, there's an interval of uncertainty in interpretation in sector 2, where values of BSR amplitudes are positive, which suggests the non-existence of BSR in this interval.

The purpose of extracting seismic amplitudes in a manual and an automatic manner is to investigate how these distinct approaches supports recognizing Bottom Simulating Reflectors. It is intuitive to consider that extracting values automatically through an interpreted horizon is more accurate, since Petrel selects wiggles associated to the same seismic event. Besides, the amplitude values are extracted for every trace number, which increases their reliability. One tremendous advantage of using the automatic approach is because this procedure consumes considerably less time than the manual way, which can be impractical in cases where the horizons are extensive.

Otherwise, as BSR can appear laterally discontinuous (Dillon et al., 1996), the automatic manner might be disregarding valid BSR amplitudes. By picking manually especially when there is a strongest reflection, despite probably not selecting values corresponding to the exact same seismic event, it is certain that the seismic amplitude corresponding to the BSR is extracted. Considering values from the seafloor amplitudes, the manual approach showed more discontinuous results (except for sections 0239-0060-2-4 and 0270-2004b that presented consistent values). This can be explained by the intervals from trace number.

Comparing the results between these two approaches, it is observed that some graphs exhibit very similar behaviors, such as for seismic section 0239-0060-2-4, 0270-2004b, but also for some intervals from sections 0239-0034 (especially between trace number 1520-1535 for sector 2, and 1336-1350 for sector 1) and 0239-0035 (1712-1720 for sector 2, and 2078-2094 for sector 1). This confrontation helps improving delineation of BSR, since in most parts where the values from BSR are negative and large is precisely when the approaches are analogous. Some differences between them were already expected, considering that during the manual procedure the values from seismic amplitudes were taken in variable intervals of trace number.

As stated in Aguiar et al. (2019), through all these graphs displayed above, the inversion in polarity between the seafloor (positive) and the BSR (negative) is promptly noticed, except for a few points. There are portions where values from BSR amplitudes are extremely large, which helps corroborating the identification of this reflector.

BSR amplitude is greatly sensitive to small gas concentrations located below the hydrate stability zone (Holbrook et al., 2002), and some authors suggest that BSRs appear discontinuous at higher frequencies, forming a series of strong reflections that are parallel

to the seafloor but laterally discontinuous (Dillon et al., 1996). This could be a justification for the intervals in which the absolute values of seismic amplitudes between the seafloor and the BSR are dissimilar. The concentration of gas hydrates above the BSR, and of free gas below it, alters and causes the intensity of the reflector to vary locally (Freire et al., 2011). Thus, the BSR will be stronger the greater the saturations of methane hydrates and free gas, which increases the impedance contrast (Aguiar et al., 2019).

6.3 Application of seismic attributes

The seismic attribute applied to the section was the Envelope (or instantaneous amplitude). As this attribute is directly related to the acoustic impedance contrast, its application is significant for the characterization of methane hydrates. Figures 21, 22, 23 and 24 show sections 0239-0035, 0239-0034, 0239-0060-2-4 and 0270-2004b with the Envelope attribute applied and possible portions of the BSR not interpreted (top) and interpreted (bottom). Location map of these seismic sections can be seen in Figures 6-9.

The use of the Envelope attribute enhances the visualization and identification of BSR, since this attribute works as a good discriminator for lithological and stratigraphic changes in reservoirs and accumulations of gas and fluids (Taner, 1992; Chen & Sidney, 1997), therefore it highlights the presence of free gas trapped beneath the BSR.

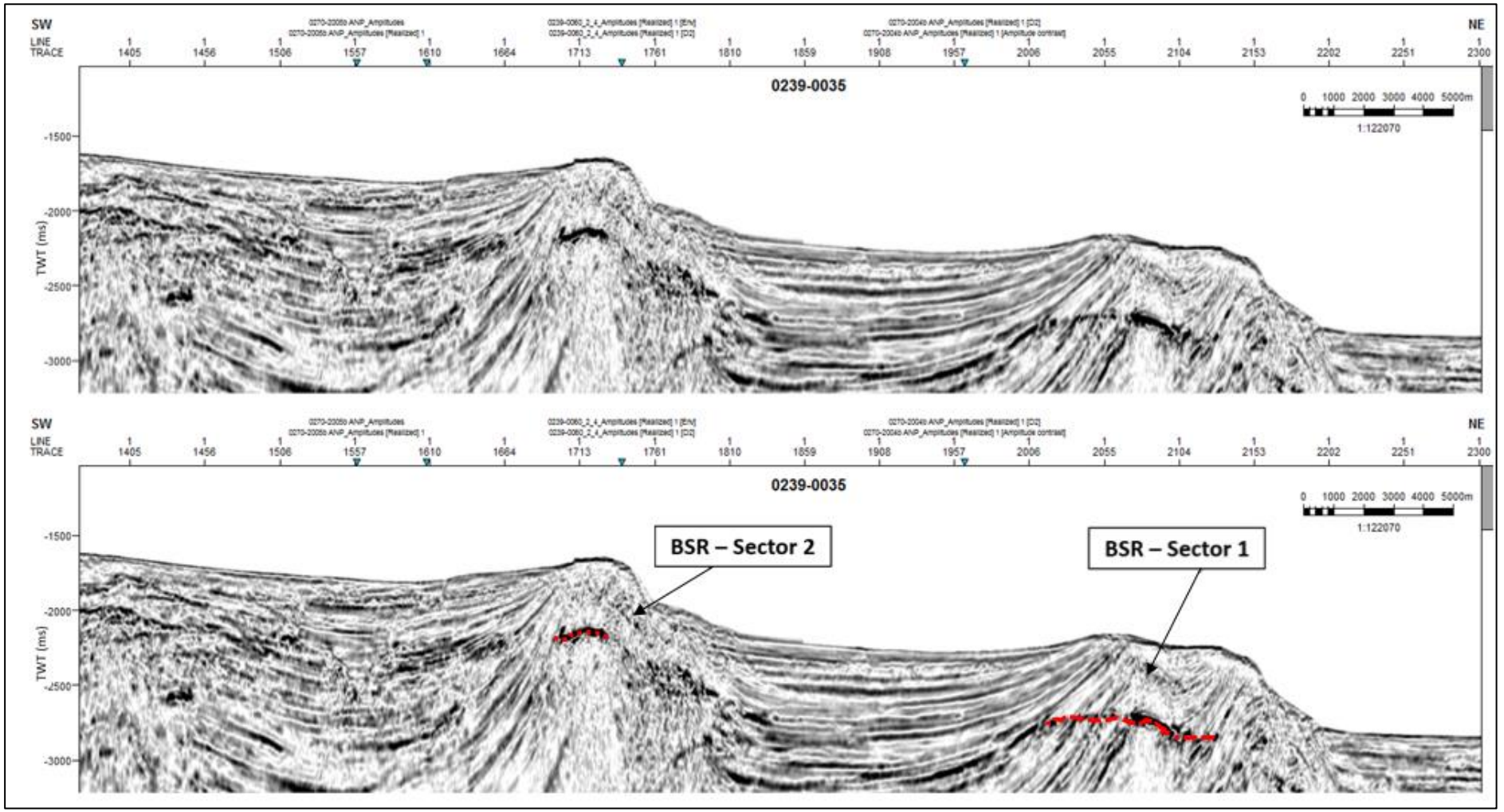

Figure 21: Seismic section 0239-0035 with Envelope attribute applied. The two sectors interpreted as BSR are highlighted in red.

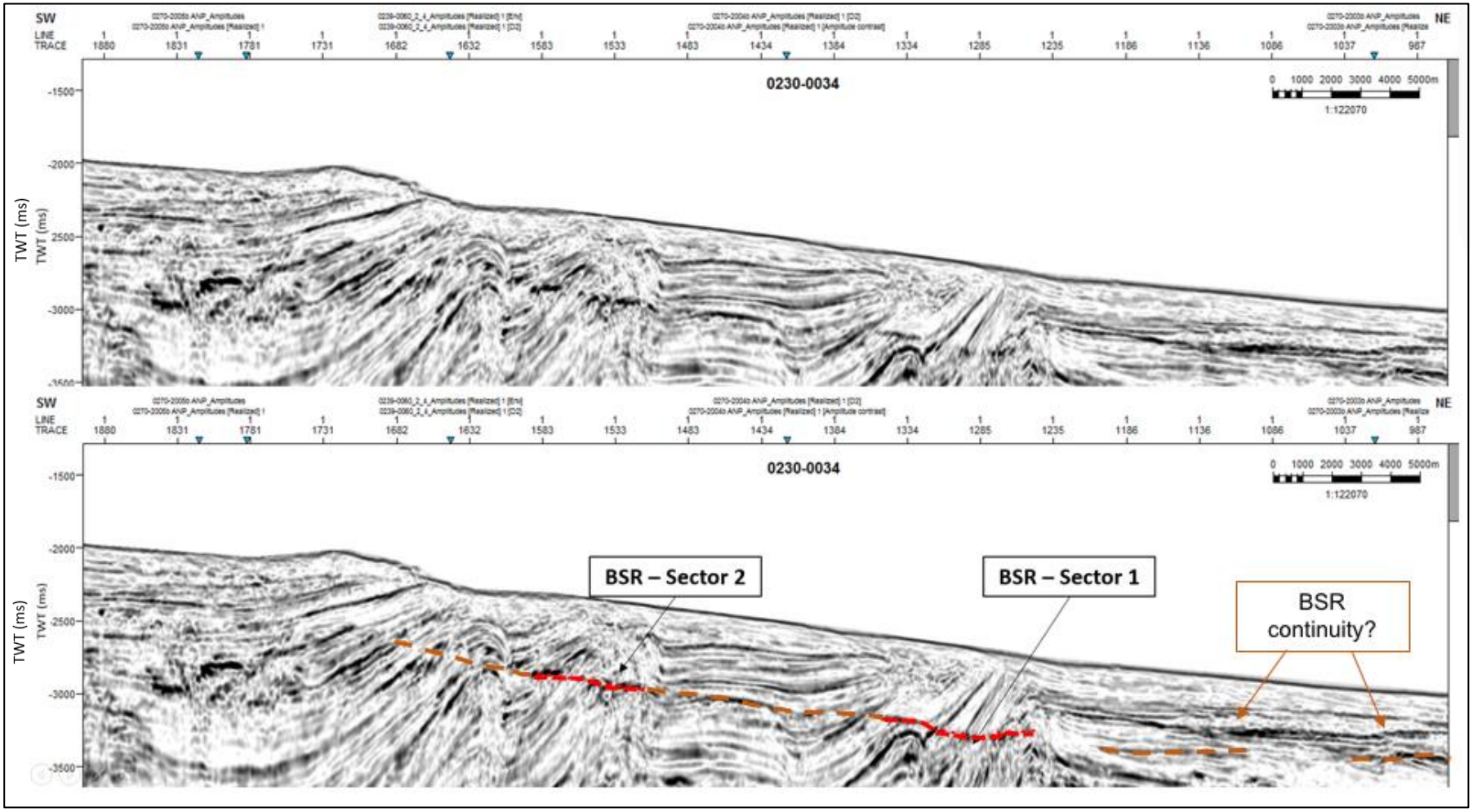

Figure 22: Seismic section 0239-0034 with Envelope attribute applied. The two sectors interpreted as BSR are highlighted in red. The interpretation in orange consists of a new possibility for BSR continuity that attribute Envelope made possible.

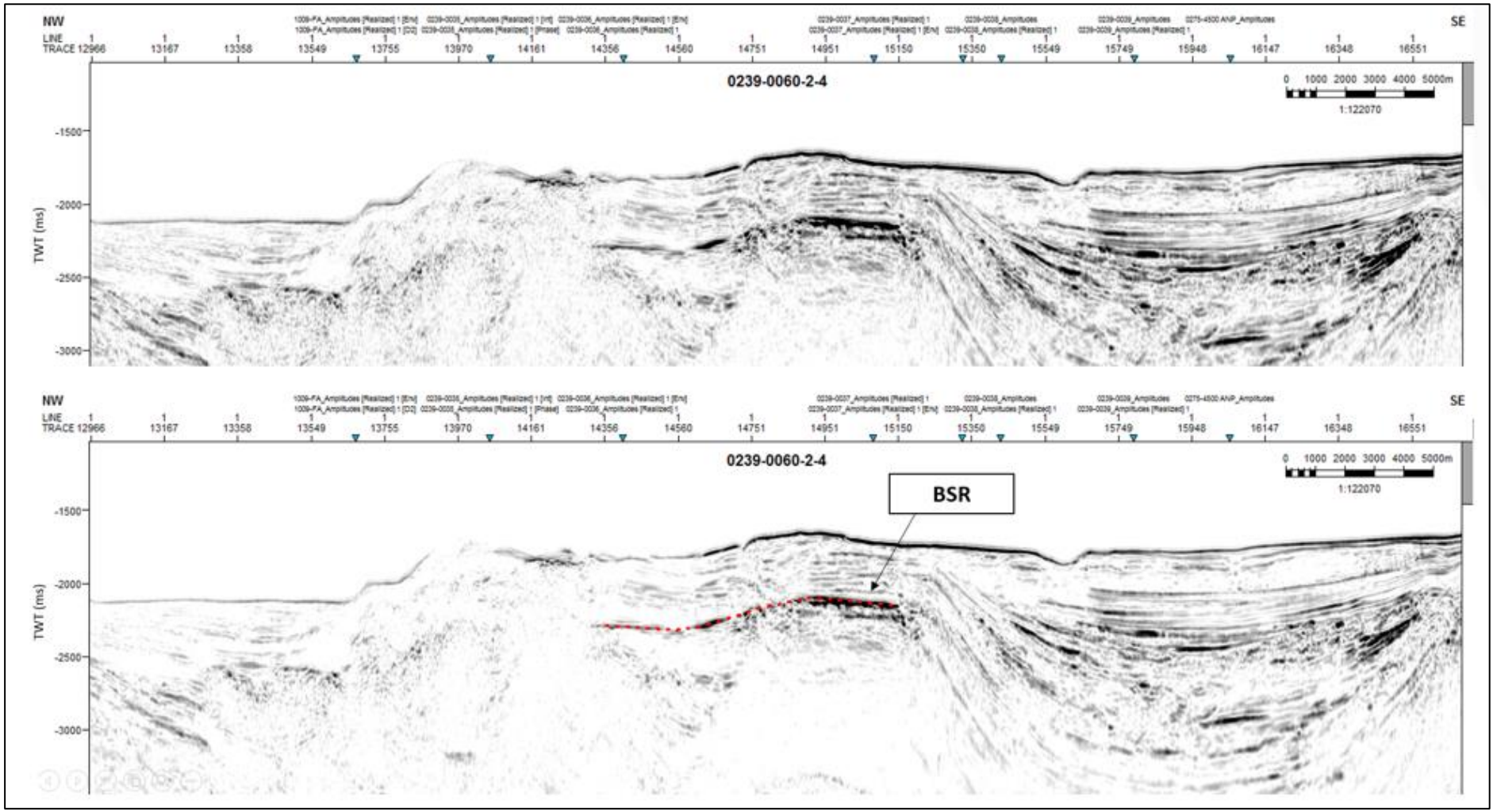

Figure 23: Seismic section 0239-0060-2-4 with Envelope attribute applied. The sector interpreted as BSR is highlighted in red.

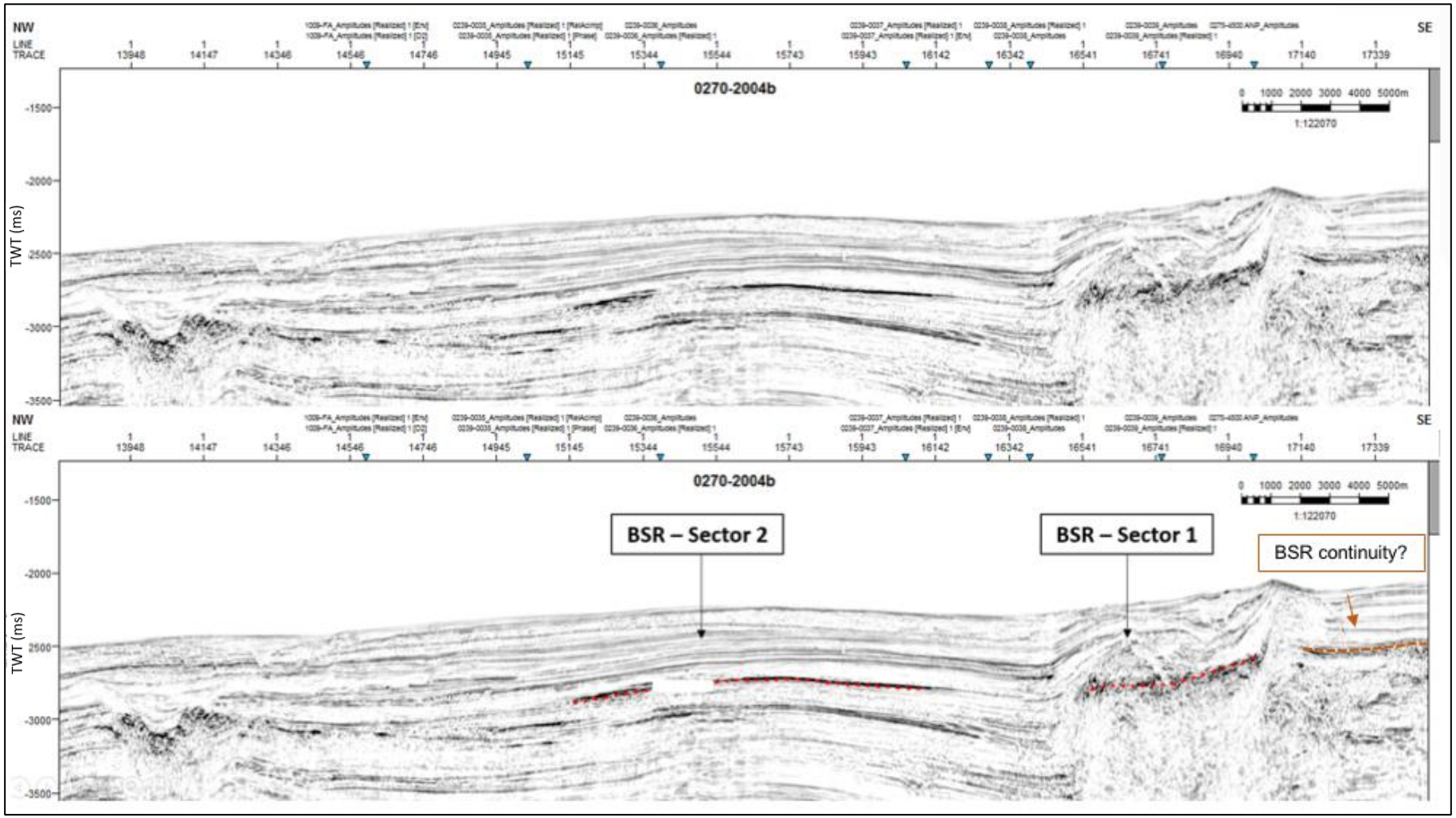

Figure 24: Seismic section 0270-2004b with Envelope attribute applied. The two sectors interpreted as BSR are highlighted in red. The sector interpreted in orange represents a new possibility for BSR continuity that attribute Envelope made possible.

It is notable from the figures above that the attribute Envelope was, as expected, successful on reinforcing the strongest reflections, and also brought light to new possibilities for BSR interpretation. However, the application of this attribute did not accentuate the portions where the interpreted BSR was not well marked, which could underestimate the potential of these methane reserves. This is probably related to the lower concentrations of gas hydrates within the hydrate stability zone and of free gas below this zone, which as mentioned before, causes the intensity of the reflector to vary locally (Freire et al., 2011).

6.4 Spectral Decomposition

During this method, seismic data in time is decomposed in different frequency bands. Before applying this attribute, a frequency spectrum was made in order to investigate the best frequency bands that might represent methane hydrates reservoir. Figure 25 shows four graphs containing the frequency spectra from each seismic section in this study.

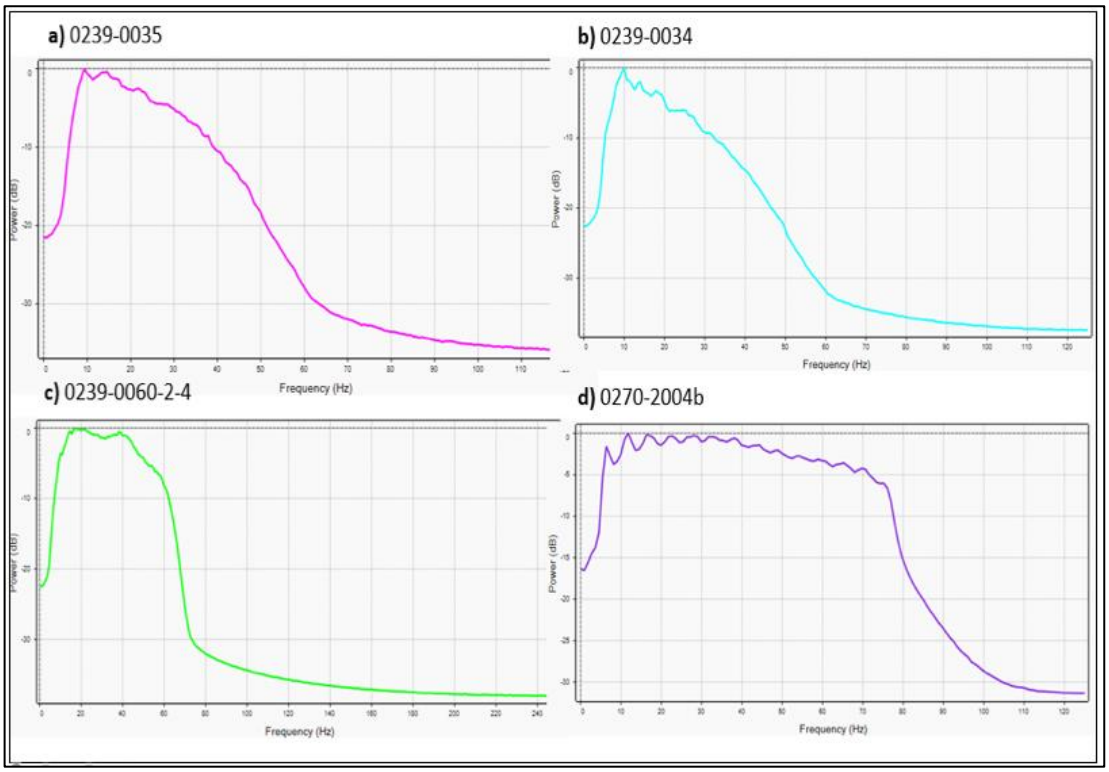

Figure 25: Frequency spectra for each seismic section.

A virtual cropping of the seismic sections was made as an attempt to select only the frequency bands that includes the BSR and, therefore, potential gas hydrates reserves. For seismic line 0239-0035, the time interval choosen for the cropping was -1500 to -3000ms; for section 0239-0034, the interval was chosen between -1900 and -3400ms; -1600 to -2700ms for line 0239-0060-2-4, and from -2000 to -3100ms for seismic section 0270-2004b.

Through these graphs displayed above, four frequency bands filters were chosen: 10Hz, 20Hz, 30HZ and 40Hz. Higher frequency bands were also applied but did not present fine results. The following Figures 26, 27, 28 and 29 show seismic section 0239-0035 with each frequency band.

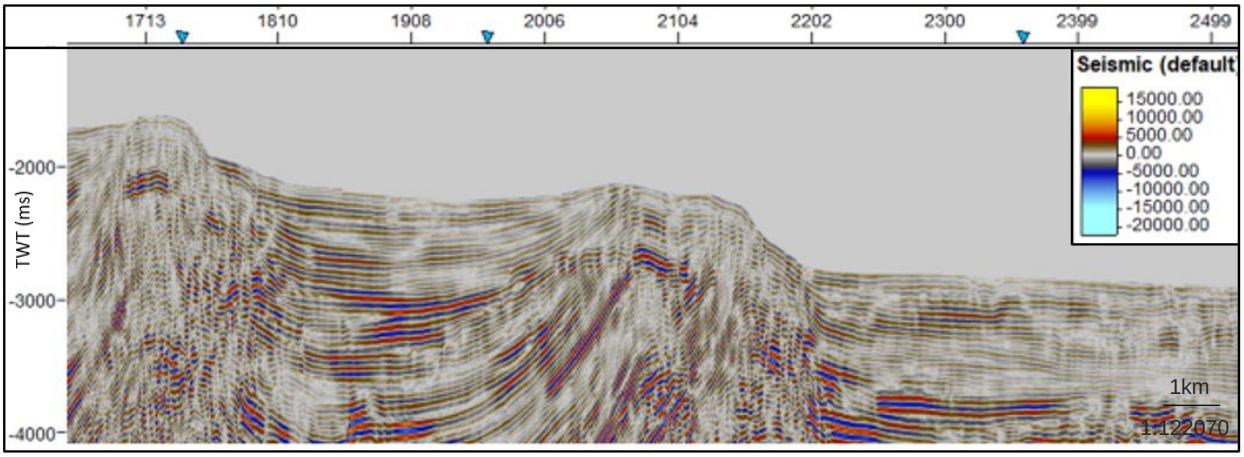

Figure 26: Seismic section 0239-0035 with 10Hz filter.

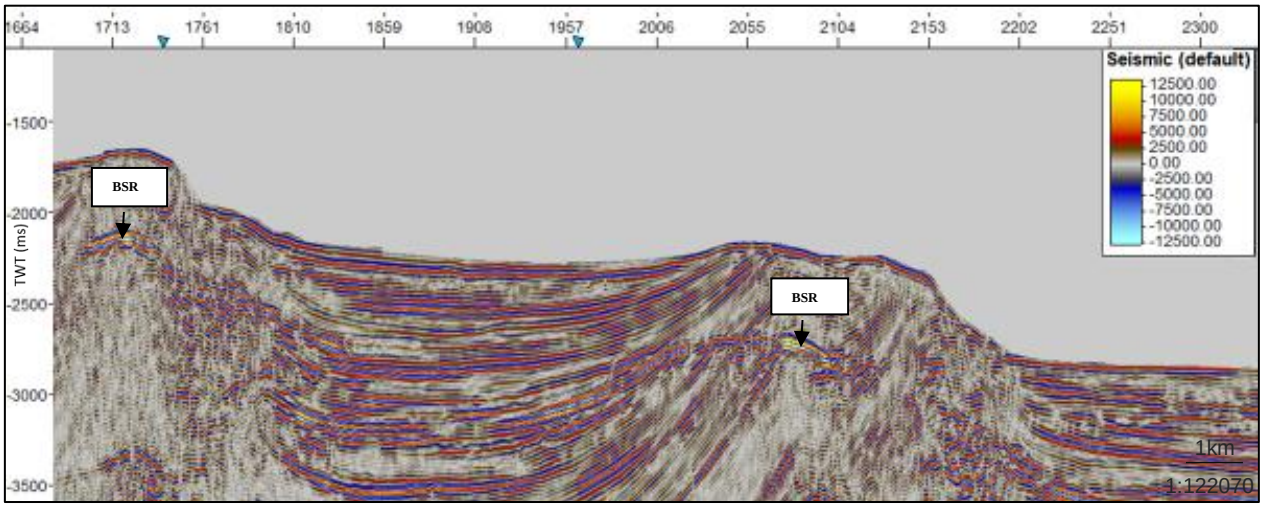

Figure 27: Seismic section 0239-0035 with 20Hz filter.

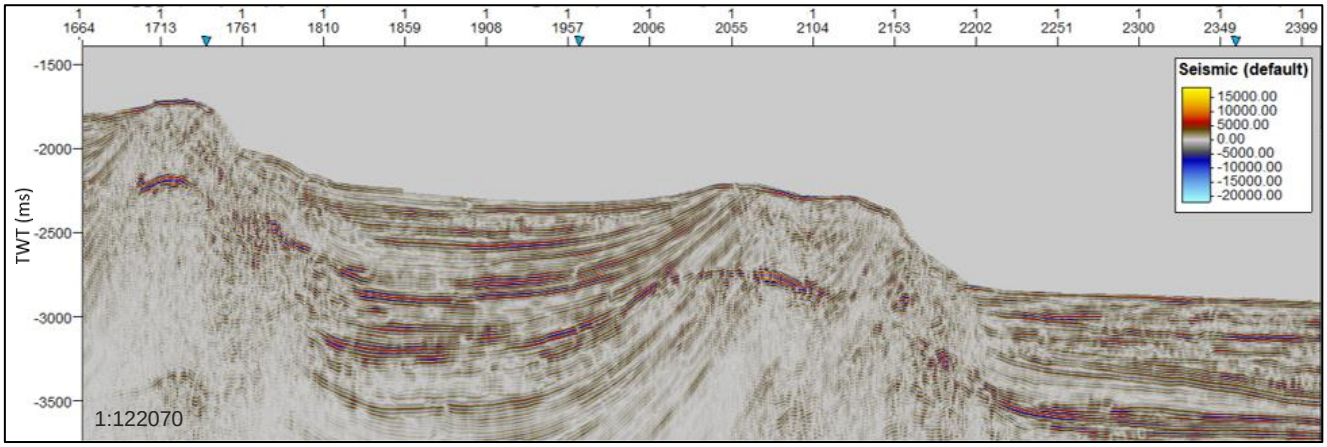

Figure 28: Seismic section 0239-0035 with 30Hz filter.

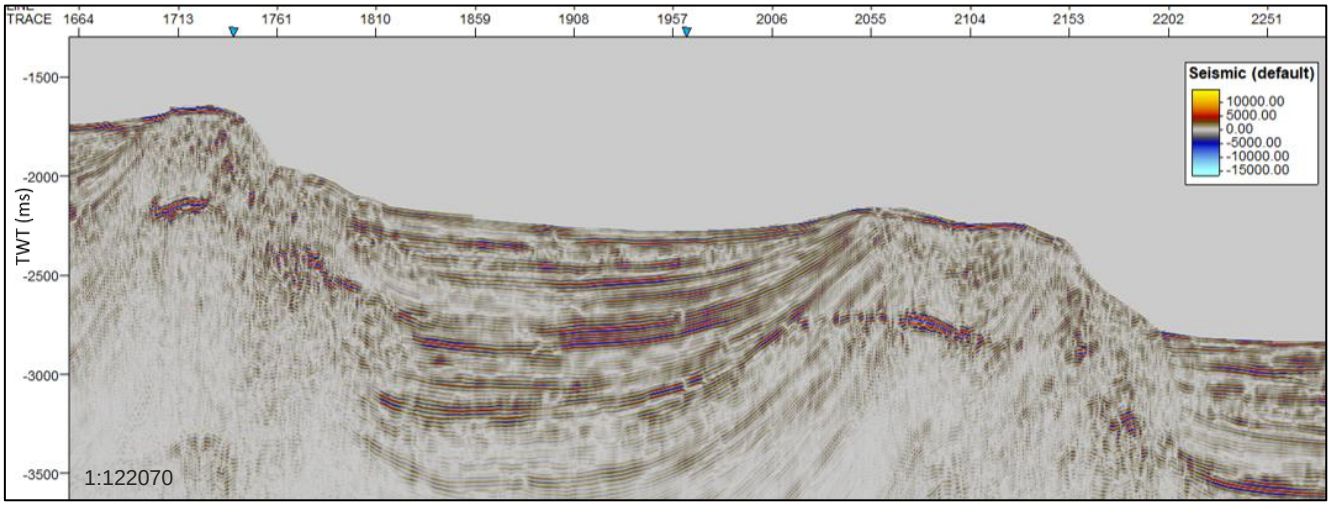

Figure 29: Seismic section 0239-0035 with 40Hz filter.

Firstly, applying Spectral Decomposition (SD) with 10Hz was not useful for interpretation in any of the seismic sections, therefore these results will not be shown in this study. By interpreting the figures above for section 0239-0035, it was possible to identify some interesting features for the other frequency bands (20Hz, 30Hz and 40Hz). As frequency band increases, the BSR is enhanced, and its discontinuity becomes more evident (see Figure 29). By using SD in different frequencies, it was possible to better delineate the bottom simulating reflector.

Figure 30 shows seismic section 0239-0035 with Envelope applied for 20Hz, 30Hz and 40Hz frequency bands.

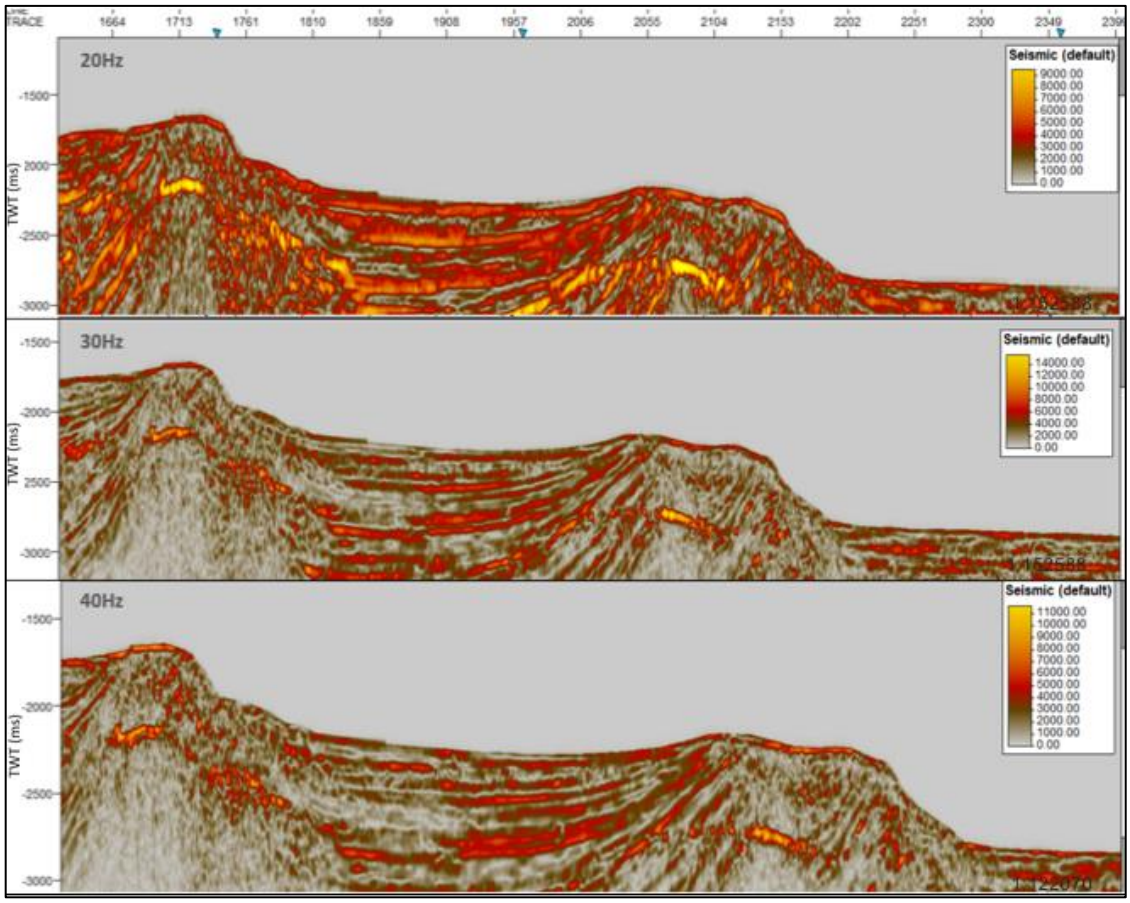

Figure 30: Seismic section 0239-0035 with Envelope applied for 20Hz, 30Hz and 40Hz frequency bands. Since this attribute is directly related to acoustic impedance contrast, its application was able to highlight BSR, especially for 20Hz, where BSR was extremely enhanced.

For seismic sections 0239-0034, 0239-0060-2-4 and 0270-2004b, since they present similar results for frequency bands 30Hz and 40Hz, and to optimize the results showed in this dissertation, there will be exhibited only two frequency bands for each seismic line. Figures 31 to 36 represent the results from spectral decomposition for these sections, along with the attribute Envelope applied:

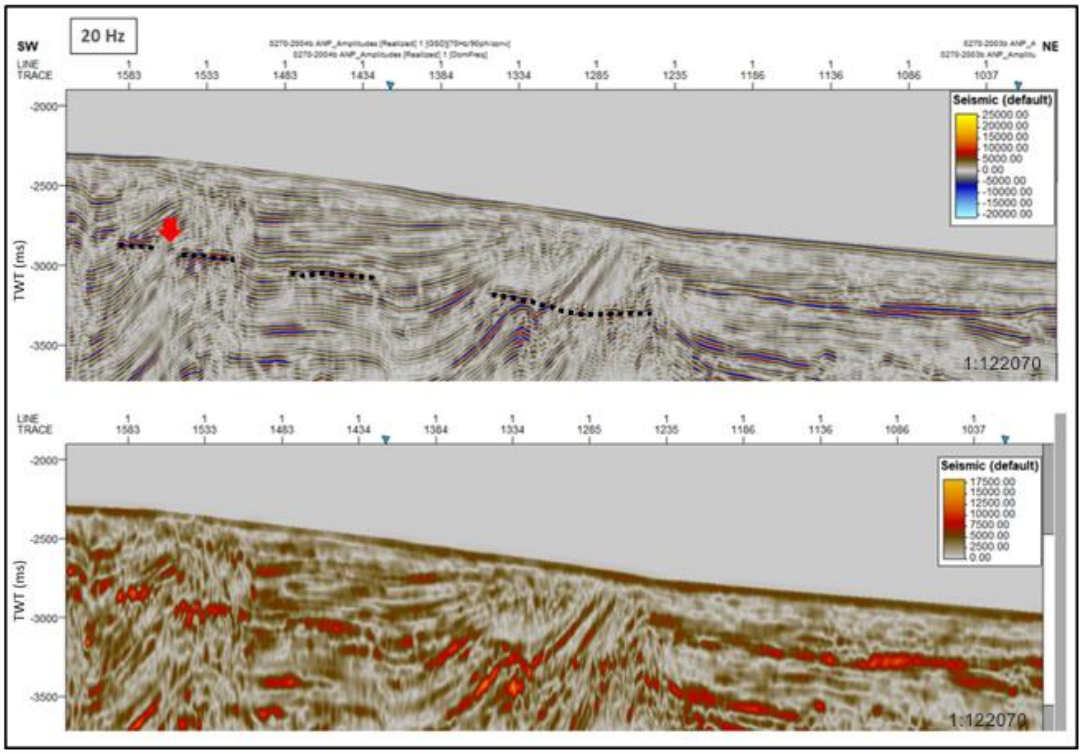

Figure 31: Seismic section 0239-0034 with 20Hz (top) and with Envelope applied (bottom). The sectors interpreted as BSR are highlighted in black. The red arrow indicates a discontinuity of BSR that became more evident after applying Spectral Decomposition.

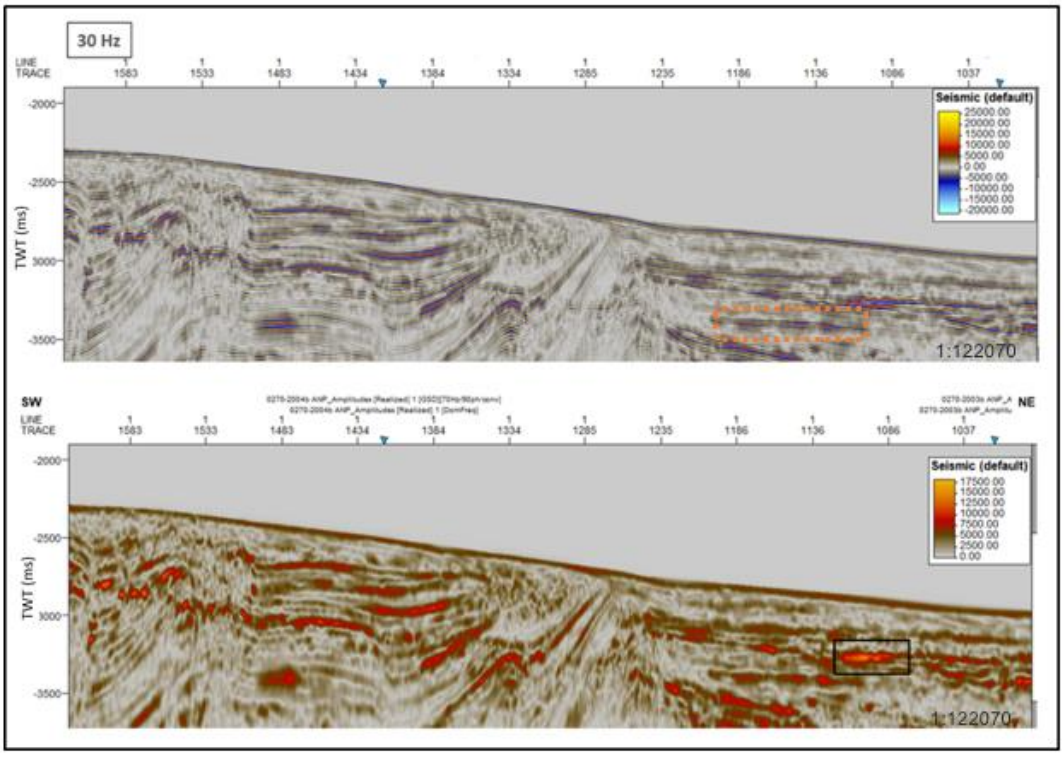

Figure 32: Seismic section 0239-0034 with 30Hz (top) and with Envelope applied (bottom). Highlighted in black there is probably a zone within the GHSZ where the saturation of free gas is higher. In orange (top), it is possible to validate the interpretation of a new continuity of BSR that was also observed after the application of Envelope.

Methane hydrates reservoirs are only generated once there are an amount of water and gas in order to create them (Freire, 2010). If there is still gas but no longer enough water to combine and to produce gas hydrates, then the hydrates might work as a seal, forming a barrier that retains gas within the gas hydrate stability zone. This could be an explanation for portions that were intensely enhanced by using spectral decomposition with Envelope, such as observed in Figure 32.

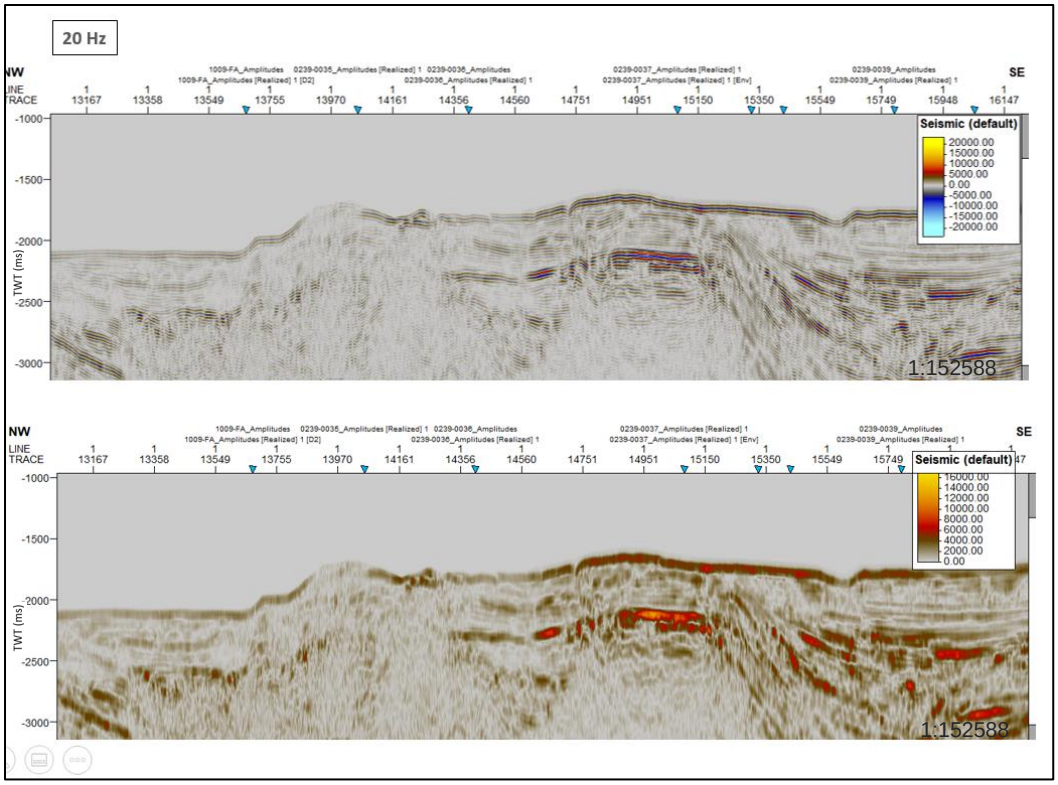

Figure 33: Seismic section 0239-0060-2-4 with 20Hz (top) and with Envelope applied (bottom). The use of Envelope enhanced the identification of BSR.

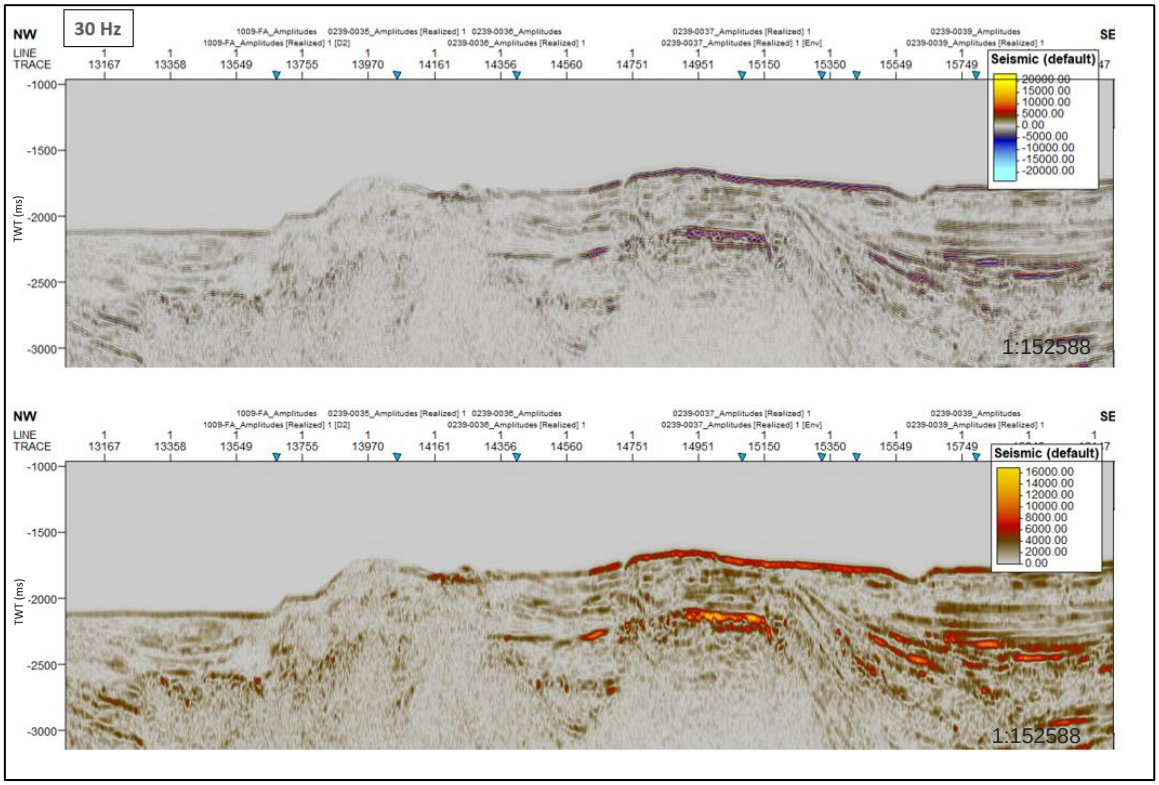

Figure 34: Seismic section 0239-0060-2-4 with 30Hz (top) and with Envelope applied (bottom).

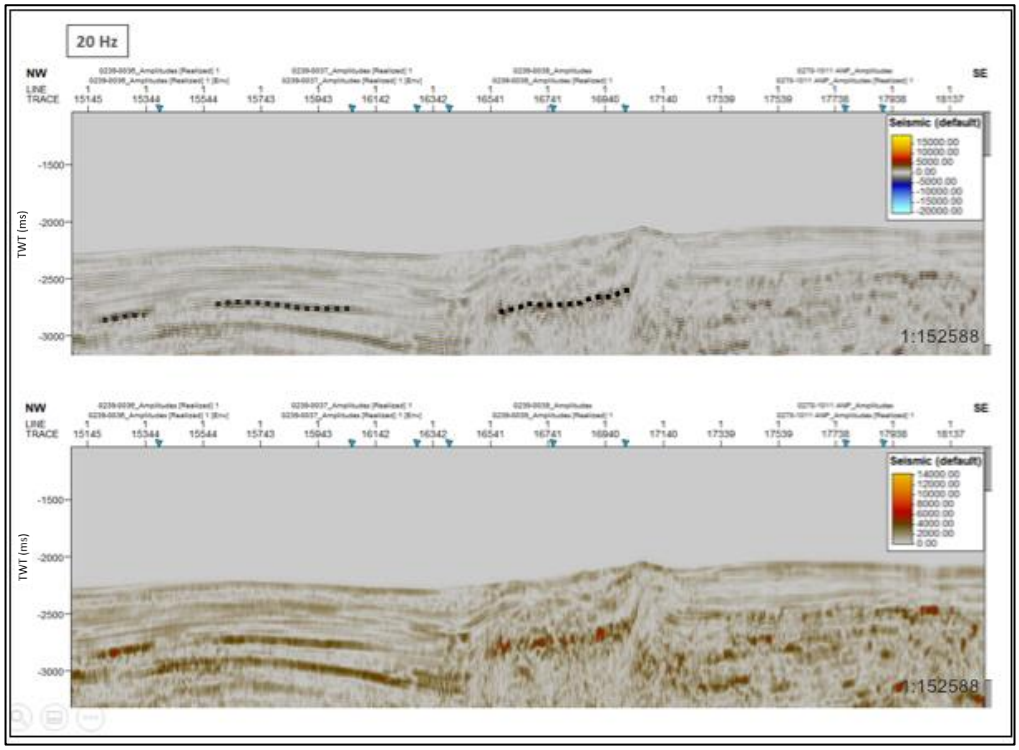

Figure 35: Seismic section 0270-2004b with 20 Hz (top) and with Envelope applied (bottom). BSR is highlighted in black. Lateral discontinuity of BSR can be noticed in the two sectors.

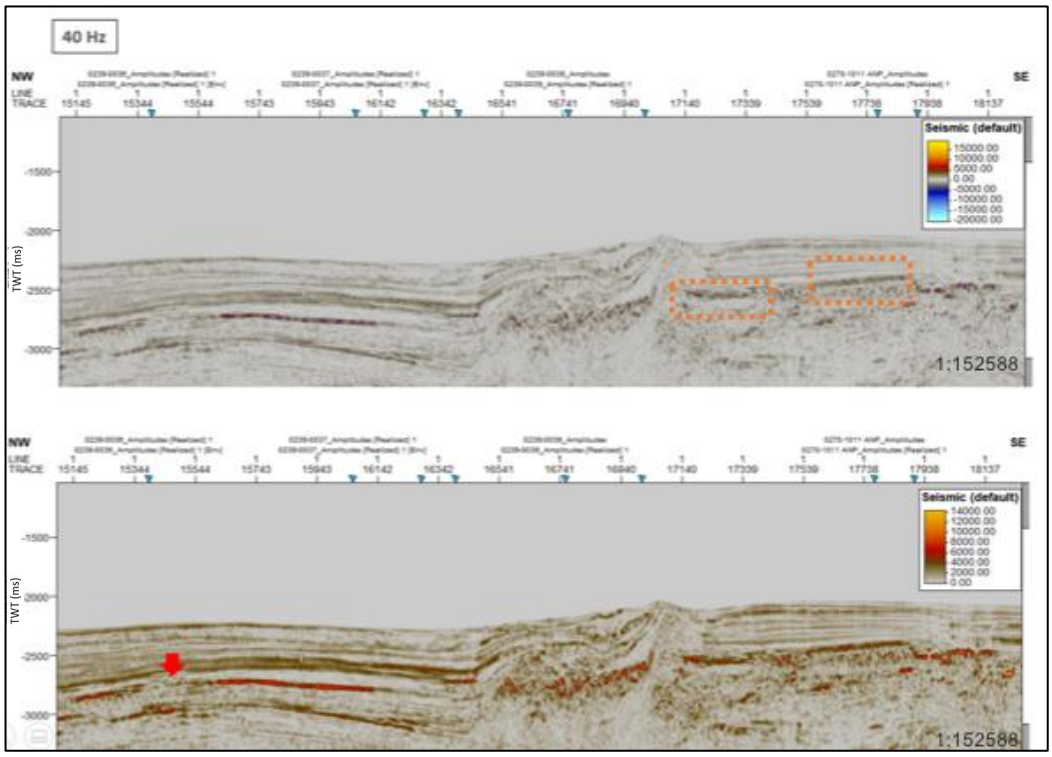

Figure 36: Seismic section 0270-2004b with 40Hz (top) and with Envelope applied (bottom). The red arrow indicates a portion where lateral discontinuity of BSR is observed. In orange (top), it is highlighted new possibilities of BSR continuity that was also noticed after the application of Envelope.

The application of attributes Generalized Spectral Decomposition and Envelope aided enrich interpretation, especially because they contributed to identify portions where BSR is laterally discontinuous and portions where new possibilities on BSR continuity are enhanced, which was seen with attribute Envelope previously. They also highlighted the free gas trapped beneath the BSR and enhanced portions where methane hydrates probably work as seals, such as observed for seismic section 0239-0034.

Besides, there is no pattern in these four seismic sections in which frequency bands helped improving BSR, although 30Hz-40Hz showed fine results.

As Satyavani et al. (2008) pointed out, mapping a BSR in a seismic section is a valid approach in order to find the occurrence of methane hydrates. There are some studies around the world in which the BSRs are simply not recognized, however gas hydrates have been confirmed by drilling (Satyavani et al., 2008). This suggests the importance of looking for other indirect methods to ascertain the presence of gas hydrates

and free gas. Therefore, utilizing seismic attributes as a tool for seismic interpretation of methane hydrates is a valid approach.

Each seismic attribute has its own advantages, disadvantages and limitations. It is worth noting the significance of applying more than one attribute for reducing uncertainties and avoiding biased interpretations. For instance, Coren et al. (2001) suggested a multi-attribute analysis with well logs correlation that supported delineate some of the characterizing physical properties of the BSR. As Satyavani et al. (2008) indicate, the application of AVO (amplitude versus offset) can also provide information about the presence of free gas beneath the BSR. However, for this is necessary a seismic survey carried on for specifically study shallow gas hydrates.

Besides, in other studies, it was observed that seismic attribute analysis allowed instantaneous amplitude (or Envelope) and instantaneous frequency sections to validate the level of the BSR (Satyavani et al., 2008; Joshi et al., 2017). Additionally, Oliveira (2009) and Oliveira et al. (2010) used spectral decomposition to identify seismic features related to methane hydrates in Pelotas Basin, such as low frequency blackout zone, blanking and gas flow, and therefore to infer the presence of gas hydrate layer and free gas. These approaches corroborate with what has been proposed in this study.

7 CONCLUSIONS

The integration of geophysical methods is valuable for an accurate characterization of the subsurface. In this study, four approaches were proposed based on seismic interpretation: firstly, identification of negative amplitude reflections as BSR; manual and automatic comparison of seismic amplitudes, and finally the application of seismic attributes and spectral decomposition, which together addressed the identification of BSR. These approaches reveal to be a useful tool for interpreting the distribution of the gas hydrates in the Foz do Amazonas Basin and can be used in other similar sites.

The results for all the four sections showed that there is an inversion of polarities in the signal between the seafloor (positive polarity) and the BSR (negative polarity), although this inversion is not always in absolute values. In addition, the attribute Envelope chosen for this study was able to enhance the visualization of BSR for the different sections, especially within frequency bands 30Hz-40Hz. Spectral decomposition helped identify portions where BSR is laterally discontinuous, additionally to highlighting portions where methane hydrates work as seals, retaining free gas within the GHSZ. The combined use of these methods allowed validating the identification of the BSR in sections 0239-0035, 0239-0034, 0239-0060-2-4 and 0270-2004b and inferring the presence of methane hydrates, even though its distribution is not continuous.

8 REFERENCES

AGUIAR, LF., FREIRE, AFM., SANTOS, LA., DOMINGUEZ, ACF., NEVES, EHP., SILVA, CG., & SANTOS, MAC. 2019. Analysis of seismic attributes to recognize bottom simulating reflectors in the Foz do Amazonas Basin, Northern Brazil. Revista Brasileira de Geofísica, 37(1), 1-11.

ARAÚJO EFS, SILVA CG, REIS ATD, PEROVANO R, GORINI C, VENDEVILLE BC & ALBUQUERQUE NCD. 2009. Movimentos de massa multiescala na bacia da Foz do Amazonas-Margem Equatorial Brasileira. Brazilian Journal of Geophysics, 27(3): 485–508.

AZEVEDO, R. P. Tectonic evolution of Brazilian equatorial margin basins. University of London, London, Tese de doutorado não publicada, 1991.

BERRYMAN J, KEARNS H, RODRIGUEZ K. 2015. Foz do Amazonas Basin—a case for oil generation from geothermal gradient modelling. First Break 33:91–95.

BRANDÃO, JAS & FEIJÓ, FJ. 1994. Bacia da Foz do Amazonas. Boletim de Geociências da Petrobras, 8(1): 91–99.

BRUNO, G. Argilocinese no Cone do Amazonas. 1987. 103 f. Dissertação (Mestrado em Geologia) – Universidade Federal de Ouro Preto – Ouro Preto, MG, 1987.

CANARIO, RS. 2013. Avaliação de Atributos Sísmicos utilizados no reconhecimento de Hidratos de Gás no Cone do Amazonas. 90 p. Trabalho de Conclusão de Curso (Bacharelado em Geofísica) – LAGEMAR. Universidade Federal Fluminense – Niterói, RJ.

CARVALHO GCRD. 2008. Interpretação sísmica e modelagem física do cone do Amazonas, Bacia da Foz do Amazonas, margem equatorial brasileira. Master's dissertation. Departamento de Geologia, Escola de Minas, Universidade Federal de Ouro Preto, MG, Brazil. 119 pp.

CASTAGNA JP, SUN S, SIEGFRIED RW. 2003. Instantaneous spectral analyses: detection of low-frequency shadows associated with hydrocarbons. Leading Edge 22:120–127.

CHEN Q & SIDNEY S. 1997. Seismic attribute technology for reservoir forecasting and monitoring. The Leading Edge, 16(5): 445–448.

CHONG, Z. R.; YANG, S. H. B.; BABU, P.; LINGA, P.; LI, X. S. 2016. Review of natural gas hydrates as an energy resource: Prospects and challenges. Applied Energy, v. 162, p. 1633-1652.

CHOPRA S & MARFURT KJ. 2005. Seismic attributes - A historical perspective. Geophysics, 70(5): 3SO–28SO.

CLENNELL, M. B. Hidrato de Gás Submarino: Natureza, Ocorrência e Perspectivas Para Exploração na Margem Continental Brasileira. Revista Brasileira de Geofísica. Vol. 18, n. 3, 2000.

COBBOLD PR, MOURGUES R & BOYD K. 2004. Mechanism of thin-skinned detachment in the Amazon Fan: assessing the importance of fluid overpressure and hydrocarbon generation. Marine and Petroleum Geology, 21(8): 1013–1025.

COREN F, VOLPI V & TINIVELLA U. 2001. Gas hydrate physical properties imaging by multi-attribute analysis – Blake Ridge BSR case history. Marine Geology, 178(1-4): 197–210.

DAMUTH JE & KUMAR N. 1975. Amazon cone: morphology, sediments, age, and growth pattern. Geological Society of America Bulletin, 86(6): 863–878.

DILLON WP, HUTCHINSON DR & DRURY RM. 1996. Seismic reflection profiles on the Blake Ridge near Sites 994, 995, and 997. In: Proceedings of the Ocean Drilling Program. Initial Reports, 164: 47-56.

FIGUEIREDO, JJP, ZALÁN, PV & SOARES EF. 2007. Bacia da Foz do Amazonas. Boletim de Geociências da Petrobras, 15(2): 299–309.

FLOOD RD & PIPER DJ. 1997. Amazon Fan sedimentation: the relationship to Equatorial climate change, continental denudation, and sea-level fluctuations. In: FLOOD RD, PIPER DJW, KLAUS A & PETERSON LC (Eds.). Proceedings of the Ocean Drilling Program. Scientific Results, 155: 653–675.

FREIRE AFM. 2010. An integrated study on the gas hydrate area of Joetsu Basin, eastern margin of Japan Sea, using geophysical, geological and geochemical data. Ph.D. thesis. Graduate School of Frontier Sciences. The University of Tokyo, Japan. 247 pp.

FREIRE AFM. 2013. Controle estrutural-estratigráfico na distribuição de hidratos e gases livres do anticlinal Umitaka, Bacia Joetsu, margem leste do Mar do Japão. 2013. Boletim de Geociências da Petrobrás. Maio de 2013.

FREIRE, AFM. 2017. Recursos Petrolíferos Não-Convencionais – Aula 09: Hidratos de Gás. Niterói, RJ. 91 p. Notas de aula.

FREIRE AFM, MATSUMOTO R & SANTOS LA. 2011. Structural-stratigraphic control on the Umitaka Spur gas hydrates of Joetsu Basin in the eastern margin of Japan Sea. Marine and Petroleum Geology, 28: 1967–1978.

GEHRMANN R, MÜLLER C, SCHIKOWSKY P, HENKE T, SCHNABEL M & BÖNNEMANN C. 2009. Model-based Identification of the Base of the Gas Hydrate Stability Zone in Multichannel Reflection Seismic Data, Offshore Costa Rica. International Journal of Geophysics, 2009: ID 812713, 12 pp.

HATO M, MATSUOKA T, INAMORI T, SAEKI T. 2006. Detection of methane-hydrates bearing zones using seismic attributes. Leading Edge 25:607–609.

HOLBROOK WS, GORMAN AR, HOMBACH M, HACKWITH KL, NEALON J, LIZARRALDE D & PECHER IA. 2002. Seismic detection of marine methane hydrate. The Leading Edge, 21(7): 686–689.

HOVLAND, M.; JUDD, A.G. Focus on North Sea Pockmarks. In: Hovland, M. & Judd, A.G. (eds.). Seabed Pockmarks and Seepages: Impact on Geology, Biology and the Marine Environment. Graham & Trotman, London, UK. Cap. 2, p. 6-34, 1988.

HYNDMAN RD & SPENCE GD. 1992. A seismic study of methane hydrate marine bottom simulating reflectors. Journal of Geophysical Research: Solid Earth, 97(B5): 6683–6698.

JOSHI AK, PANDEY L & SAIN K. 2017. Identification of BSR and estimation of gas hydrate from well-log data at NGHP-01-04a and 11A in the Krishna-Godavari Basin, Eastern Indian Margin. In: SEG Technical Program Expanded Abstracts 2017. Society of Exploration Geophysicists. p. 3483–3487.

KATZMAN R, HOLBROOK WS & PAULL CK. 1994. Combined vertical-incidence and wide-angle seismic study of a gas hydrate zone, Blake Ridge. Journal of Geophysical Research: Solid Earth, 99(B9): 17975–17995.

KETZER JM, AUGUSTIN A, RODRIGUES LF, OLIVEIRA R, PRAEG D, PIVEL MAG, DOS REIS AT, SILVA C & LEONEL B. 2018. Gas seeps and gas hydrates in the Amazon deep-sea fan. Geo-Marine Letters, 38(5): 429–438.

KVENVOLDEN KA. 1993. Gas hydrates-geological perspective and global change. Reviews of Geophysics, 31(2): 173–187.

KVENVOLDEN KA. 1998. A primer on the geologic occurrence of gas hydrate. In: Henriet, J. P. and J. Mienert, eds., Gas hydrates: relevance to world margin stability and climate change: Geol. Soc. London, Special Publications, v. 137, p. 9, 1998.

LEE MW, HUTCHINSON DR, DILLON WP, MILLER JJ, AGENA WF, SWIFT BA. 1993. Method of estimating the amount of in situ gas hydrates in deep marine sediments. Mar Pet Geology 10:493–506.

LIU, G., FOMEL, S., & CHEN, X. 2011. Time-frequency analysis of seismic data using local attributes. Geophysics, 76(6), P23-P34.

LORENSON TD & KVENDOLVEN KA. 2001. A worldwide Assessment of Coincidental gas hydrate and Petroleum Gas Occurrences. In: AAPG Annual Convention. Program with Abstracts, Tulsa, AAPG, v. 10, A120.

MANLEY PL, FlOOD RD. 1988. Cyclic sediment deposition within Amazon deep-sea fan. Am Assoc Petrol Geol Bull 72:912–925.

MASLIN M & MIKKELSEN N. 1997. Amazon Fan mass-transport deposits and underlying interglacial deposits: age estimates and Fan dynamics. In: FLOOD RD, PIPER DJW, KLAUS A & PETERSON LC (Eds.). Proceedings of the Ocean Drilling Program. Scientific Results, 155: 353–365.

MASLIN M, VILELA C, MIKKELSEN N & GROOTES P. 2005. Causes of catastrophic sediment failures of the Amazon Fan. Quaternary Science Reviews, 20: 2180–2193.

MCCONNELL, D. R.; KENDALL, B. A. Images of the Base of Gas Hydrate Stability, Northwest Walker Ridge, Gulf of Mexico. Offshore Technology Conference. v. 10, 4043/14103-MS, 2002.

MILLER DJ, KETZER JM, VIANA AR, KOWSMANN RO, FREIRE AFM, OREIRO SG, AUGUSTIN AH, LOUREGA RV, RODRIGUES LF, HEEMANR & PREISSLER AG. 2015. Natural gas hydrates in the Rio Grande Cone (Brazil): A new province in the western South Atlantic. Marine and Petroleum Geology, 67: 187–196.

OJHA M & SAIN K. 2009. Seismic attributes for identifying gas-hydrates and free-gas zones: application to the Makran accretionary prism. Episodes, 32(4): 264–270.

OLIVEIRA, OMV. 2009. Decomposição espectral de dados sísmicos usando a transformada de wavelet: aplicação no estudo das acumulações de hidratos de gás na bacia de Pelotas. 2009. 60 p. Dissertação (Mestrado em Engenharia de Reservatório e de Exploração de Petróleo) – Universidade Estadual do Norte Fluminense, Macaé, RJ.

OLIVEIRA, S. OLIVEIRA, OMV. & Da Costa, E. 2010. Time–frequency spectral signature of Pelotas Basin deep water gas hydrates system. Marine Geophysical Researches, 31(1-2), 89-97.

PARTYKA G, GRIDLEY J, LOPEZ JA. 1999. Interpretational applications of spectral decomposition in reservoir characterization. Leading Edge 18:353–360.

PASLEY MA, SHEPHERD DB, POCKNALL DT, BOYD KP, ANDRADE V & FIGUEIREDO JP. 2004. Sequence stratigraphy and basin evolution of the Foz do Amazonas Basin, Brazil. In: AAPG International Conference & Exhibition. Cancun, Mexico: American Association of Petroleum Geologists, 10082.

PAULL, C.K.; USSLER III, W.; BOROWSKI, W.S. Sources of methane to form marine gas hydrates, Annals of New York Academy of Sciences, v. 715, p. 392-409, 1994.

PINTAS, EM. 2011. Análise de Atributos AVO e Física de Rochas Aplicados na Identificação e Caracterização de Hidratos de Gás na Bacia de Pelotas. 79 f. Trabalho de Conclusão de Curso (Bacharelado em Curso de Geofísica) - LAGEMAR, UFF, Rio de Janeiro, 2011.

PIPER DJW, PIRMEZ C, MANLEY PL, LONG D, FLOOD RD, NORMARK WR & SHOWERS W. 1997. Mass-transport deposits of the Amazon Fan. In: FLOOD

RD, PIPER DJW, KLAUS A & PETERSON LC (Eds.). Proceedings of the Ocean Drilling Program. Scientific Results, 155: 109–146.

REIS AT, PEROVANO R, SILVA CG, VENDEVILLE BC, ARAÚJO E, GORINI C & OLIVEIRA V. 2010. Two-scale gravitational collapse in the Amazon Fan: a coupled system of gravity tectonics and mass-transport processes. Journal of the Geological Society, 167(3): 593–604.

REIS AT, ARAÚJO E, SILVA CG, CRUZ AM, GORINI C, DROZ L, MIGEON S, PEROVANO R, KING I & BACHE F. 2016. Effects of a regional décollement level for gravity tectonics on late Neogene to recent large-scale slope instabilities in the Foz do Amazonas Basin, Brazil. Marine and Petroleum Geology, 75: 29–52.

RIMINGTON N, CRAMP A & MORTON A. 2000. Amazon Fan sands: implications for provenance. Marine and Petroleum Geology, 17(2): 267–284.

ROSA, M.L.C.C.; R.N., AYUP-ZOUAIAN, R.N.; BARBOZA, E.G. 2006. Utilização de Seções Sísmicas 2D na identificação de Zonas de Escapes de Fluidos. Gravel, Porto Alegre, n. 4, p. 109-118.

RUSSEL BH. 2004. The application of multivariate statistics and neural networks to the prediction of reservoir parameters using seismic attributes. Ph.D. thesis. University of Calgary, Canada. 392 pp.

SAD ARE, SILVEIRA DP, MACHADO MAP, SILVA SRP & MACIEL RR (Eds.). 1998. Marine gas hydrates evidence along the Brazilian Coast. In: AAPG International Conference and Exhibition. Rio de Janeiro, Brazil: American Association of Petroleum Geologists.

SATYAVANI N, SAIN K, LALL M & KUMAR BJP. 2008. Seismic attribute study for gas hydrates in the Andaman Offshore India. Marine Geophysical Researches, 29(3): 167–175.

SHIPLEY TH, HOUSTON MH, BUFFLER RT, SHAUB FJ, McMILLEN KJ, LADD JW & WORZEL JL. 1979. Seismic reflection evidence for widespread occurrence of possible gas-hydrate horizons on continental slopes and rises. American Association of Petroleum Geologists Bulletin, 63: 2204–2213.

SINGH, S.C.; MINSHULL, T.A.; SPENCE, G.D. Velocity structure of a Gas Hydrate Reflector. 1993. Science, New York, v. 260, n.5105, p. 204-207.

SLOAN Jr ED. 2003. Fundamental principles and applications of natural gas hydrates. Nature, 426(6964): 353.

SOARES Jr AV, COSTA JBS & HASUI Y. 2008. Evolução da Margem Atlântica Equatorial do Brasil: Três Fases Distensivas. Geociências (São Paulo), 27: 427–437.

STEIN JA, JOHNSON RA, CASAVANT RR, WARREN MB. 2007. Calibration and analysis of methane hydrate beneath Alaska's North Slope using spectral decomposition of 3-D seismic reflection data. American Geophysical Union, Fall Meeting, abstract #OS23A-1066.

TAI, S., PURYEAR, C., & CASTAGNA, J. P. 2009. Local frequency as a direct hydrocarbon indicator. In SEG Technical Program Expanded Abstracts 2009 (pp. 2160-2164). Society of Exploration Geophysicists.

TANAKA MD, SILVA CG, CLENNELL MB. 2003. Gas hydrates on the Amazon Submarine Fan, Foz do Amazonas Basil, Brazil. AAPG Search and Discovery Article #90013, AAPG Annual Meeting, May 11–14, 2003, Salt Lake City, Utah.

TANER MT. 1992. Attributes Revisited - Rock Solid Images. Houston, Texas. RSI. (Revised Sep. 2000), p. 3-27.

TANER MT. 2001. Seismic Attributes. CSEG Recorder, 26(7): 49–56.

TANER MT, KOEHLER F & SHERIFF RE. 1979. Complex seismic trace analysis. Geophysics, 44(6): 1041–1063.

TANER MT, O'DOHERTY R, SCHUELKE JS & BAYSAL E (Eds.). 1994. Seismic attributes revisited. In: 64th SEG Annual Meeting. Expanded Abstracts. Los Angeles, US, Society of Exploration Geophysicists.

8.1 ADDITIONAL REFERENCES

BANCO DE DADOS DE EXPLORAÇÃO E PRODUÇÃO – BDEP WebMaps, ANP. <http://webmaps.anp.gov.br/mapas/Lists/DSPAppPages/MapasBrasil.aspx; http://www.anp.gov.br/images/EXPLORACAO_E_PRODUCAO_DE_OLEO_E_GAS/DadoS_Tecnicos/autorizacoes_despachos/2005/48610.0008652005-37.pdf (accessed March 2019).

APPENDIX

Manual approach

(Tables containing amplitude data picked manually from seafloor and BSR for the four seismic sections)

- Seismic amplitudes of the seafloor and the BSR on sector 1 (0239-0035) – Manual approach:

0239-0035 - Sector 1					
Trace number	Seafloor	BSR - Sector 1	Trace number	Seafloor	BSR - Sector 1
2112	12808.56	-10656.72	2058	3621.08	-4828.11
2110	9941.59	-16342.33	2056	6595.07	-8324.93
2108	9742.86	-7887.07	2054	8689.13	-7888.82
2106	6571.67	-3447.43	2052	1334.79	-1557.25
2104	10053.42	-13246.86	2050	10097.24	-12217.66
2102	12520.13	-10762.92	2048	7923.26	-7923.26
2100	12471.26	-12270.68	2046	9508.13	-7253.63
2098	10451.69	-17781.45	2044	7316.68	-11405.42
2096	3333.18	-3199.85	2042	6146.11	-10243.5
2094	11625.4	-17576.5	2040	7663.14	-6583.83
2092	10089.71	-16173.21	2038	7079.82	-14687.98
2090	9656.11	-6025.84	2036	8147.05	-6449.75
2088	10560.94	-11979.57	2034	6858	-464.95
2086	11739.3	-20389.32	2032	5955.43	-5382.79
2084	10566.54	-18044.4	2030	4629.75	-3105.9
2082	11348.44	-15924.43	2028	4401.63	-2475.91
2080	10307.38	-18287.28	2026	4463.05	-1580.67
2078	9845.25	-17753.72	2024	5638.22	-7301.96
2076	9757.63	-19876.65	2022	8304.45	-7932.61
2074	6618.8	-16901.58	2020	8357.59	-10103.95
2072	4437.52	-3138.74			
2070	6857.89	-12423.72			
2068	4503.11	-4102.83			
2066	3450.3	-6325.55			
2064	6168.75	-4498.05			
2062	6052.86	-13192.13			
2060	7234.5	-11795.37			

- Seismic amplitudes of the seafloor and the BSR on sector 2 (0239-0035) – Manual approach**:**

0239-0035 - Sector 2					
Trace number	Seafloor	BSR - Sector 2	Trace number	Seafloor	BSR - Sector 2
1732	8220.2	-2901.25	1700	8542.56	-6930.76
1730	9832.01	-9993.19	1698	805.9	-1289.44
1728	9832.01	-13055.61	1696	4835.41	-4513.05
1726	8381.38	-13377.98	1694	6769.58	-1450.62
1724	5480.13	-12249.71	1692	4835.41	-1289.44
1722	13055.61	-17891.03	1690	2095.35	-2256.53
1720	12088.53	-18858.11	1688	8220.2	-2578.89
1718	9026.1	-8220.2	1686	7253.12	-6286.04
1716	12894.43	-12733.25	1684	7414.3	-4351.87
1714	10315.55	-14345.06	1682	7575.48	-3868.33
1712	12894.43	-19825.19	1680	3868.33	-3223.61
1710	10315.55	-19341.65	1678	6769.58	-3545.97
1708	12410.89	-11766.17	1676	6447.22	-3707.15
1706	9832.01	-11443.81	1674	9026.1	-4835.41
1704	9187.28	-15956.86	1672	7414.3	-7091.94
1702	10154.37	-13216.79			

- Seismic amplitudes of the seafloor and the BSR on sector 1 (0239-0034) – Manual approach.

0239-0034 - Sector 1					
Trace number	Seafloor	BSR - Sector 1	Trace number	Seafloor	BSR - Sector 1
1260	9072.16	-6294.97	1310	6109.82	-7961.28
1265	9812.74	-11108.76	1315	4443.51	-9812.74
1270	9072.16	-7590.99	1320	2036.61	-185.15
1275	9072.16	-8331.57	1325	8887.01	-8146.43
1280	8887.01	-1296.02	1330	12404.79	-10738.47
1285	4443.51	-1666.31	1335	10923.62	-8146.43
1290	9627.59	-8887.01	1340	11293.91	-11108.76
1295	11108.76	-7776.13	1345	6109.82	-5924.67
1300	8516.72	-5184.09	1350	4813.8	-7509.99
1305	11849.35	-2592.04	1355	9257.3	-2221.75

- Seismic amplitudes of the seafloor and the BSR on sector 2 (0239-0034) – Manual approach.

0239-0034 - Sector 2					
Trace number	Seafloor	BSR - Sector 2	Trace number	Seafloor	BSR - Sector 2
1515	4998.94	-1666.31	1555	10738.47	-10368.18
1520	13885.95	-12219.64	1560	9257.3	-3147.48
1525	12960.22	-10368.18	1565	8331.57	-4628.65
1530	10378.47	-15922.56	1570	7590.99	-9812.74
1535	5554.38	-5554.38	1575	10183.03	-12960.22
1540	9072.16	-10923.62	1580	6850.4	-18514.61
1545	12589.93	-13885.95	1585	7405.84	-7509.99
1550	7961.28	-4073.21	1590	3517.78	-2592.04

- Seismic amplitudes of the seafloor and the BSR (0239-0060-2-4) – Manual approach.

0239-0060-2-4								
Trace number	Seafloor	BSR	Trace number	Seafloor	BSR	Trace number	Seafloor	BSR
14320	6665,29	-4628,7	14550	5184,11	-4998,97	14680	9627,64	-7591,02
14325	740,59	-925,73	14555	5739,55	-4813,82	14685	1296,03	-1666,32
14330	3332,64	-1851,5	14560	4813,82	-3332,64	14690	4998,97	-925,73
14335	5924,7	-4528,4	14565	6294,99	-5369,26	14695	9072,2	-555,44
14440	4813,82	-7591	14570	1666,32	-1110,88	14700	2962,35	-370,29
14445	5924,7	-6295	14575	185,15	-555,44	14705	5184,11	-1296,03
14450	6480,14	-5924,7	14580	4628,67	-2036,62	14710	3332,64	-2406,91
14455	5369,26	-6480,1	14585	2036,62	-2036,62	14715	3332,64	-4998,97
14460	4813,82	-5369,3	14590	4443,52	-2962,35	14720	3517,79	-6294,99
14465	5924,7	-5184,1	14595	4998,97	-4443,52	14725	2406,91	-1481,18
14470	5369,26	-4628,7	14600	6480,14	-6109,85	14230	7405,88	-7220,73
14475	1666,32	-2406,9	14605	2777,2	-6109,85	14235	7591,02	-12404,84
14480	1296,03	-5369,3	14610	3147,5	-10533,37	14740	7035,58	-10183,08
14485	2036,62	-6850,4	14615	4628,67	-11479,11	14745	9442,49	-9257,34
14490	3517,79	-7220,7	14620	4628,67	-14256,31	14780	740,59	1666,32
14495	4998,97	-6480,1	14625	8887,05	-9627,64	14785	8331,61	-1666,32
14500	4258,38	-6295	14630	6294,99	-10368,22	14790	1666,32	-2221,76
14505	5554,41	-5184,1	14635	7405,88	-15737,48	14795	5369,26	-4813,82
14510	4998,97	-4999	14640	14996,9	-17774,1	14800	7405,88	-1851,47
14515	4258,38	-4813,8	14645	12589,99	-15182,04	14805	8887,05	-2777,2
14520	4258,38	-3702,9	14650	14441,46	-14256,31	14810	6850,43	-3517,79
14525	3332,64	-3332,6	14655	14996,9	-12034,55	14815	3517,79	-2962,35
14530	3517,79	-3888,1	14660	13515,72	-13700,87	14820	6665,29	-4073,23
14535	4258,38	-3517,8	14665	11108,81	-12034,55	14825	8331,61	-2221,76
14540	3702,94	-3888,1	14670	9627,64	-9627,64	14830	5184,11	-3147,5
14545	4443,52	-2962,4	14675	8146,46	-9627,64	14835	8887,05	-5554,41

0239-0060-2-4								
Trace number	Seafloor	BSR	Trace number	Seafloor	BSR	Trace number	Seafloor	BSR
14840	6480,14	-7591	14970	17218,66	-17218,66	15100	18144,39	-22587,92
14845	8701,9	-4628,7	14975	14626,6	-14626,6	15105	12404,84	-13700,87
14850	2406,91	-3517,8	14980	17403,81	-17033,51	15110	15737,48	-11293,96
14855	4073,23	-3702,9	14985	16663,22	-15367,19	15115	10183,08	-20736,45
14860	4258,38	-3888,1	14990	19070,13	-17588,95	15120	16848,37	-21106,74
14865	6109,85	-4443,5	14995	19810,71	-20736,45	15125	17774,1	-20921,6
14870	4998,97	-7035,6	15000	19995,86	-22402,77	15130	14071,16	-13886,02
14875	3517,79	-9072,2	15005	13515,72	-22587,92	15135	18884,98	-13515,72
14880	10183,08	-8701,9	15010	11293,96	-14256,31	15140	14996,9	-12404,84
14885	10368,22	-9442,5	15015	14256,31	-15182,04	15145	15367,19	-13515,72
14890	9812,78	-7405,9	15020	12404,84	-13700,87	15150	14626,6	-10368,22
14895	4813,82	-7035,6	15025	16478,07	-13515,72			
14900	7776,17	-5184,1	15030	13330,58	-11849,4			
14905	8331,61	-6850,4	15035	14626,6	-16663,22			
14910	12960,28	-8701,9	15040	14811,75	-16107,78			
14915	12034,55	-8331,6	15045	17403,81	-15552,34			
14920	14071,16	-11849	15050	14071,16	-13145,43			
14925	12589,99	-15923	15055	19255,28	-16292,92			
14930	14996,9	-16478	15060	13515,72	-14071,16			
14935	13515,72	-14627	15065	16663,22	-15182,04			
14940	13886,02	-15737	15070	12960,28	-14996,9			
14945	17033,51	-16848	15075	15552,34	-15737,48			
14950	17959,25	-14627	15080	15922,63	-16663,22			
14955	15737,48	-10368	15085	19995,86	-17033,51			
14960	17959,25	-17034	15090	14811,75	-13330,58			
14965	17774,1	-16663	15095	17959,25	-20181,01			

- Seismic amplitudes of the seafloor and the BSR on sector 1 (0270-2004b) – Manual approach.

0270-2004b - Sector 1								
Trace number	Seafloor	BSR - Sector 1	Trace number	Seafloor	BSR - Sector 1	Trace number	Seafloor	BSR - Sector 1
16535	6097	-5315,34	16665	3595,67	-3752	16795	3595,67	-7504,01
16540	6566	-5159	16670	-6409,67	4533,67	16800	3439,34	-13601,01
16545	1407	-4377,34	16675	4690	-1563,33	16805	3908,34	-6097
16550	3752	-3595,67	16680	4221	-3752	16810	2657,67	-7035,01
16555	6097	-5315,34	16685	4221	-1563,33	16815	3439,34	-3752
16560	5002,67	-7660,34	16690	3595,67	-9223,67	16820	2814	-7035,01
16565	6566	-5159	16695	3908,34	-3908,34	16825	4846,34	-11881,34
16570	4221	-7191,34	16700	4064,67	-6253,34	16830	2032,33	-8442,01
16575	5159	-3752	16705	4064,67	-5628	16835	4377,34	-7816,67
16580	2970,34	-4064,67	16710	4846,34	-2345	16840	781,67	-5471,67
16585	3752	-15789,68	16715	2657,67	-12506,68	16845	2657,67	-3595,67
16590	2032,33	-5940,67	16720	1876	-14539,01	16850	781,67	-2032,33
16595	3595,7	-3752	16725	2657,67	-8598,34	16855	4377,34	-5940,67
16600	938	-2188,67	16730	1563,33	-7660,34	16860	3908,34	-4846,34
16605	3126,67	-6097	16735	2345	-6566	16865	3595,67	-3752
16610	4846,34	-2657,67	16740	-11881,34	3283	16870	4846,34	-5628
16615	4377,34	-3439,34	16745	2032,33	-2032,33	16875	1876	-4064,67
16620	2032,33	-781,67	16750	2345	-1563,33	16880	2814	-1719,67
16625	2657,67	-2501,34	16755	1250,67	-4533,67	16885	2501,34	-7504,01
16630	1563,33	-1094,33	16760	4064,67	-6722,34	16890	4846,34	-3752
16635	3126,67	-2188,67	16765	1876	-781,67	16895	5159	-6253,34
16640	3126,67	0	16770	4064,67	-2501,34	16900	4064,67	-6097
16645	1876	-4846,34	16775	1563,33	-2188,67	16905	4221	-3752
16650	1876	-5159	16780	2032,33	-781,67	16910	3439,34	-5315,34
16655	2501,34	-2188,67	16785	1094,33	-4377,34	16915	2501,34	-7347,67
16660	938	-6253,34	16790	1094,33	-8129,34	16920	4533,67	-10161,67

- Seismic amplitudes of the seafloor and the BSR on sector 2 (0270-2004b) – Manual approach.

0270-2004b - Sector 2											
Trace number	Seafloor	BSR - Sector 2	Trace number	Seafloor	BSR - Sector 2	Trace number	Seafloor	BSR - Sector 2	Trace number	Seafloor	BSR - Sector 2
15625	5628	-13288,34	15755	5784,34	-5159	15895	7035,01	-4221	16025	7504,01	-12194,01
15630	4377,34	-9067,34	15760	5315,34	-13913,68	15900	6253,34	-15789,68	16030	6722,34	-11568,67
15635	5315,34	-9692,67	15765	5002,67	-8598,34	15905	6409,67	-10943,34	16035	7816,67	-9849,01
15640	5002,67	-9223,67	15770	5315,34	-8129,34	15910	6253,34	-17353,01	16040	8285,67	-8911,01
15645	5159	-17040,35	15775	5159	-14695,34	15915	6566	-7191,34	16045	8285,67	-6409,67
15650	5940,67	-8285,67	15780	3439,34	-2814	15920	5940,67	-14851,68	16050	7347,67	-14226,34
15655	6253,34	-8598,34	15785	4064,67	-14070,01	15925	5159	-4533,67	16055	6097	-12194,01
15660	6722,34	-8911,01	15790	6566	-12194,01	15930	7035,01	-13601,01	16060	6409,67	-8911,01
15665	7347,67	-11725,01	15795	5628	-10318,01	15935	7191,34	-11256,01	16065	5940,67	-13444,68
15670	4221	-15008,01	15800	6097	-7660,34	15940	7816,67	-11881,34	16070	4221	-2970,34
15675	5002,67	-15946,01	15805	4533,67	-4846,34	15945	4533,67	-19385,35	16075	7347,67	-9380,01
15680	4846,34	-15477,01	15810	7035,01	-16884,01	15950	4533,67	-11725,01	16080	7504,01	-6722,34
15685	5471,67	-6097	15815	6566	-12037,68	15955	3595,67	-16571,35	16085	6097	-5940,67
15690	5002,67	-8757,67	15820	6253,34	-8911,01	15960	6409,67	-14851,68	16090	6878,67	-11881,34
15695	5002,67	-11412,34	15825	5784,34	-6722,34	15965	3126,67	-13913,68	16095	7973,01	-11725,01
15700	5315	-2657,67	15830	4690	-5471,67	15970	5940,67	-13288,34	16100	8285,67	-8754,67
15705	5628	-15320,68	15835	6409,67	-7504,01	15975	4846,34	-13757,34	16105	4846,34	-3908,34
15710	6409,67	-14695,34	15840	4846,34	-10943,34	15980	5315,34	-11099,67	16110	6722,34	-8598,34
15715	7191,34	-14070,01	15845	7504,01	-9849,01	15985	6409,67	-10474,34	16115	5940,67	-9849,01
15720	7035,01	-13132,01	15850	7816,67	-8911,01	15990	6097	-7816,67	16120	5784,34	-10161,67
15725	7504,01	-11725,01	15855	6722,34	-4221	15995	5315,34	-5471,67	16125	5159	-7816,67
15730	7191,34	-11256,01	15860	7191,34	-7660,34	16000	6097	-14382,68			
15735	7035,01	-11568,67	15865	4064,67	-12506,68	16005	6722,34	-12506,68			
15740	5315,34	-10161,67	15870	2970,34	-2970,34	16010	5471,67	-8598,34			
15745	5794,34	-9536,34	15875	6878,67	-9223,67	16015	6878,67	-7191,34			
15750	6097	-8285,67	15890	6566	-9223,67	16020	8129,34	-15633,34			